

# LGR5 as a Therapeutic Target of Antibody-Functionalized Biomimetic Magnetoliposomes for Colon Cancer Therapy

Ana Cepero <sup>1-3,\*</sup>, Mónica Jiménez-Carretero<sup>4,\*</sup>, Ylenia Jabalera<sup>4</sup>, Lidia Gago<sup>1-3</sup>, Cristina Luque<sup>1-3</sup>, Laura Cabeza <sup>1-3</sup>, Consolación Melguizo <sup>1-3</sup>, Concepcion Jimenez-Lopez<sup>4</sup>, José Prados <sup>1-3</sup>

<sup>1</sup>Institute of Biopathology and Regenerative Medicine (IBIMER), Center of Biomedical Research (CIBM), University of Granada, Granada, 18100, Spain;

<sup>2</sup>Department of Anatomy and Embryology, Faculty of Medicine, University of Granada, Granada, 18071, Spain; <sup>3</sup>Biosanitary Research Institute ibs. GRANADA, Granada, 18012, Spain; <sup>4</sup>Department of Microbiology, Sciences School, University of Granada, Granada, 18002, Spain

\*These authors contributed equally to this work

Correspondence: Laura Cabeza; Concepción Jimenez-Lopez, Email lautea@ugr.es; cjl@ugr.es

**Purpose:** The lack of specificity of conventional chemotherapy is one of the main difficulties to be solved in cancer therapy. Biomimetic magnetoliposomes are successful chemotherapy controlled-release systems, hyperthermia, and active targeting agents by functionalization of their surface with monoclonal antibodies. The membrane receptor Leucine-rich repeat-containing G-protein coupled receptor 5 (LGR5) stands out as colorectal cancer (CRC) biomarker and appears to be related to treatment resistance and the development of metastasis. The aim of this study was to assess the effectiveness and safety of LGR5-targeted biomimetic magnetoliposomes loaded with oxaliplatin (OXA) or 5-fluorouracil (5-FU) in the selective treatment of CRC and their possible application in hyperthermia.

**Methods:** Synthesis, characterization and determination of heating capacity of magnetoliposomes transporting OXA or 5-FU (with and without LGR5 functionalization) were conducted. In vitro antitumoral activity was assayed in multiple colorectal cell lines at different times of exposition. In addition to this, cell internalization was studied by Prussian Blue staining, flow cytometry and fluorescence microscopy. In vivo acute toxicity of magnetoliposomes was performed to evaluate iron-related toxicity.

**Results:** OXA and 5-FU loaded magnetoliposomes functionalized with LGR5 antibody showed higher cellular uptake than non-targeted nanoformulation with a reduction of the percentage of proliferation in colon cancer cell lines up to 3.2-fold of the IC<sub>50</sub> value compared to that of free drug. The differences between non-targeted and targeted nanoformulations were more evident after short exposure times (4 and 8 hours). Interestingly, assays in the MC38 transduced cells with reduced LGR5 expression (MC38-L(-)), showed lower cell internalization of LGR5-targeted magnetoliposomes compared to non-transduced MC38 cell line. In addition, magnetoliposomes showed an in vitro favorable heating response under magnetic excitation and great iron-related biocompatibility data in vivo.

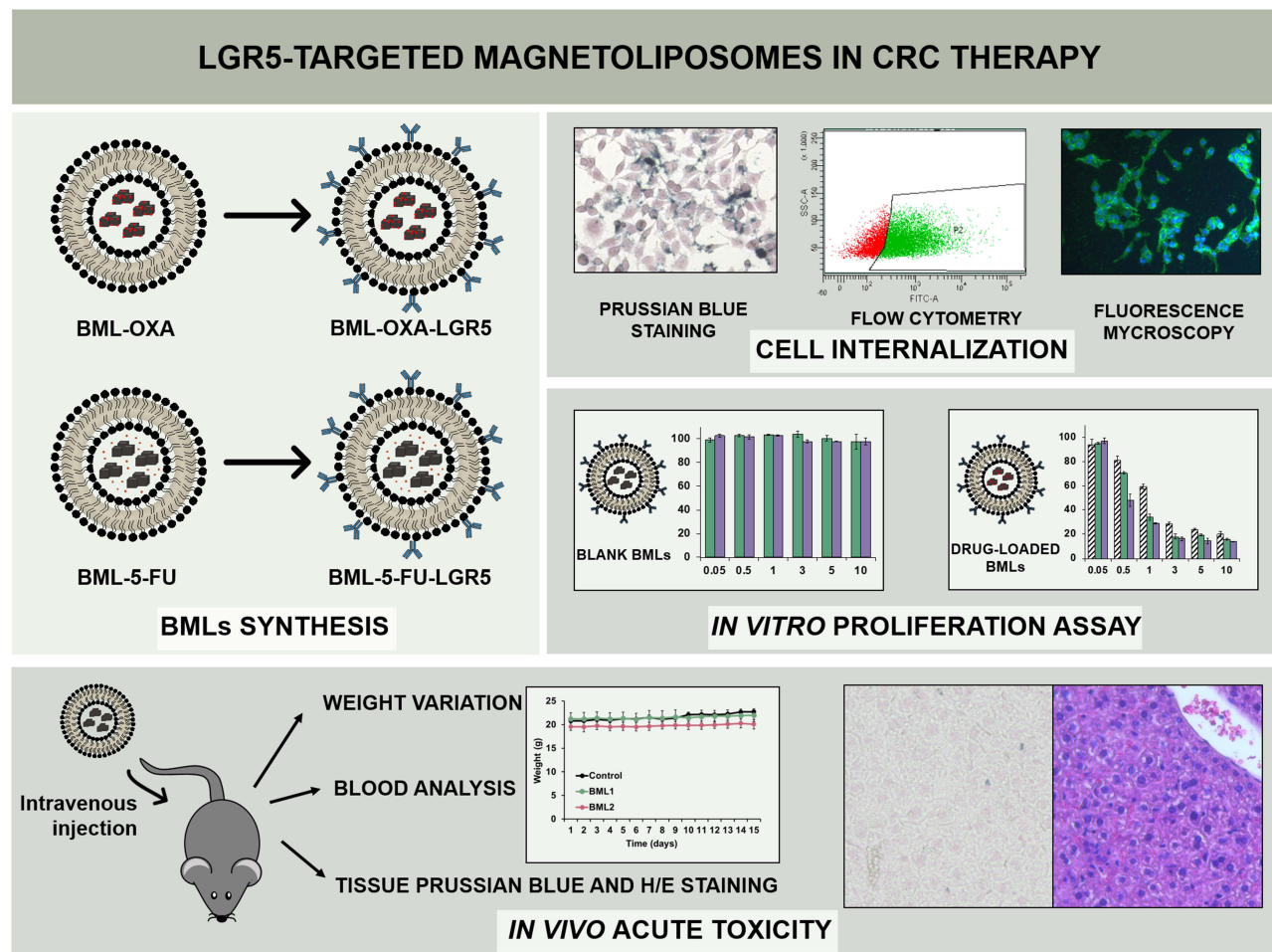
**Conclusion:** Drug-loaded magnetoliposomes functionalized with anti-LGR5 antibodies could be a promising CRC treatment strategy for LGR5+ targeted chemotherapy, magnetic hyperthermia, and both in combination.

**Keywords:** colorectal neoplasms, magnetoliposome, LGR5, oxaliplatin, 5-fluorouracil, magnetic hyperthermia

## Introduction

Conventional chemotherapy usually involves the administration of drugs with side effects outside the target tissue partly because of their lack of specificity, which leads to discontinuing pharmacological treatment and limits therapeutic success. Some of the chemotherapeutic drugs most used in the treatment of colorectal cancer (CRC), the third with the highest incidence worldwide, are oxaliplatin (OXA) and 5-fluorouracil (5-FU) usually used in combinations such as FOLFOX (5-FU/leucovorin + OXA), FOLFIRI (5-FU/leucovorin + irinotecan) and FOLFIRINOX (5-FU/leucovorin + OXA + irinotecan).<sup>1,2</sup> The most frequent adverse effects observed were peripheral sensory neuropathy, gastrointestinal

## Graphical Abstract



disorders and hematological suppression following the administration of OXA, and cardiotoxicity and myelosuppression after 5-FU treatment.<sup>3-5</sup> For this reason, the development of a new strategy of targeted therapy to the tumor tissue would allow improvement in patient's quality of life and greater adherence to treatment.

Nanomedicine could be one of these new strategies because they can overcome pharmacokinetic limitations of antitumor drugs. An important factor is the low bioavailability of chemotherapeutics caused by the electronegative surface of most of them that could be solved by their encapsulation in a nanoparticle.<sup>6</sup> In addition, nanomedicine-based drug delivery systems permit to slow down the clearance of drugs, increase the half-life, protect anticancer drugs from degradation and reduce inespecificity of cytotoxic agents in bloodstream.<sup>7,8</sup>

Due to their high surface area, nanoparticles can carry noticeable amounts of drugs, but addressing the target is also a key factor to ensure efficacy. In this context, magnetic nanoparticles have risen as plausible nanocarriers, as they can be directed employing a magnetic field. In particular, novel biomimetic nanoparticles (BMNPs) – which are synthesized by the intervention of the magnetosome-associated proteins MamC<sup>9</sup> – stand out from other types of nanoparticles. This is due to their larger size (~40 nm), which results in an enhanced magnetic moment per particle, and to the presence of MamC functional groups at the BMNP surface. This is crucial because it avoids post-production coatings and sets the isoelectric point at BMNPs to ~4.5, allowing, at physiological pH values, an electrostatic binding between the drug and BMNP and ensures the stability of the nanoassembly, while the drug is released at acidic pH values.<sup>10</sup> Moreover, BMNPs are magnetic hyperthermia agents,<sup>11</sup> thus making it possible for

therapy combination and an enhanced drug release following upon exposure to alternating magnetic fields.<sup>12</sup> Because of all these properties, BMNPs have the advantages of i) being targeted to the tumor tissue by applying an external magnetic field, ii) enhancing the antitumor effect with the combination of chemotherapy and magnetic hyperthermia, iii) being synthesized on a large scale, and iv) be biocompatible.<sup>10,13–15</sup> Specifically, OXA-conjugated BMNPs (BMNP-OXA) have been demonstrated to release OXA at acidic pH, which was potentiated by hyperthermia; in addition to a 2-fold decrease of IC<sub>50</sub> values of free OXA in CRC lines T84, HT-29, and SW480, probably due to increased cell internalization.<sup>16</sup> However, biocompatibility studies showed toxicity in macrophages that was resolved for our group by enveloping OXA-BMNP with a PEGylated unilamellar phosphatidylcholine liposome, forming a nanostructure known as magnetoliposome. Studies on OXA-BMNP-transporting PEGylated magnetoliposomes (BML-OXA) showed improved biocompatibility and cellular internalization without reducing the antitumor effects already tested in CRC cell lines.<sup>17</sup>

On the other hand, active targeting may be applied by coating magnetoliposomes with molecules – such as monoclonal antibodies,<sup>18</sup> antibody fragments,<sup>19</sup> aptamers,<sup>20</sup> etc. – that specifically recognize tumor cells.<sup>21</sup> In this context, the Leucine-rich repeat-containing G-protein coupled receptor 5 (LGR5) is a biomarker of stem-like cells in CRC, which seems to be related to resistance to radiotherapy and chemotherapy, initiation of tumor development and disease progression.<sup>22</sup> Despite numerous studies focusing on the prognostic value of LGR5, only a few have attempted to evaluate its role in CRC targeted with nanoformulations therapy such as DOX liposomes conjugated with RSPO1 – the natural ligand of LGR5 – which showed specific targeting to LGR5+ CRC cells, and a  $\approx$  4.4-fold increase in the number of apoptotic cells compared to non-targeted nanoformulation in a patient-derived xenograft tumor model of human gastric tumor.<sup>23</sup> The relevance of LGR5 as an efficient target of clinic CRC treatment has recently been supported by the use of a bispecific anti-LGR5 and EGFR antibody (MCLA-158) and autologous T cells expressing a chimeric antigen receptor (CAR) directed against LGR5 in two recent Phase I/II trials.<sup>24,25</sup>

The present study proposes a new strategy in the targeted therapy of CRC by combining the benefits of magnetoliposomes, as magnetically driven drug-carrying agents, with the possibility of targeting them to tumor tissue by receptor-mediated cellular internalization (Figure 1). The purpose of this study was to determine the effectiveness and safety of magnetoliposomes of BMNPs loaded with the drugs OXA or 5-FU and functionalized with antibodies anti-LGR5 in the selective therapy of CRC and their possible application as hyperthermia-generating agents in this tumor.

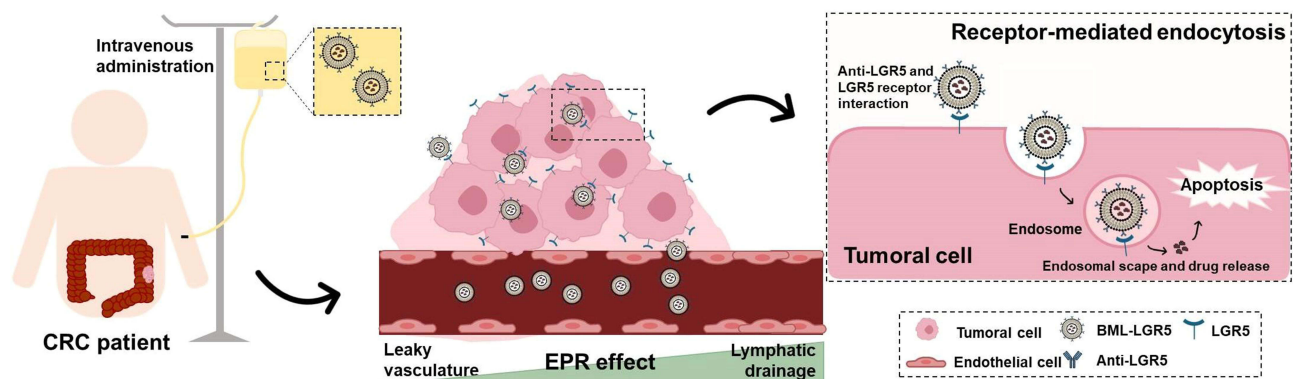


**Figure 1** Schematic representation of the suggested mechanism of action of drug-loaded magnetoliposomes targeted with anti-LGR5 antibody. Nanoformulations intravenously administered would reach the tumor by passive transport due to the enhanced permeability and retention (EPR) effect based on the formation of abnormal blood vessels and defective lymphatic drainage in solid tumors. When magnetoliposomes reach the tumor tissue anti-LGR5 antibody on magnetoliposomes surfaces specifically interacts with LGR5 tumor cell membrane receptor, and nanoformulations would be internalized by receptor-mediated endocytosis. After intracellular trafficking, the drug would be released to the cytosol leading to cell apoptosis.

## Materials and Methods

### MamC Purification and BNMPs Synthesis

MamC was produced as a recombinant protein following the protocol in Valverde-Tercedor et al.<sup>9</sup> The protein was expressed in cultures of *Escherichia coli* TOP10 growing at 37 °C (Life Technologies, Invitrogen, Grand Island, NY, USA) and induced with isopropyl- $\beta$ -D-thiogalactopyranoside (IPTG, Fisher BioReagents, Pittsburgh, PA, USA). Guanidinium lysis buffer was used to lysate the cell pellet and, after centrifugation, the supernatant was loaded onto a HiTrap chelating HP column (GE Healthcare, Chicago, IL, USA) and purified under denaturant conditions. MamC was allowed to refold by successive dialyses. All buffers were procured from Sigma Aldrich, St. Louis, MO, USA.

BMNPs were synthesized inside an anaerobic COY chamber (Coy Laboratory Products, Grass Lake, MI) from the following master solution 2.78 mM Fe(ClO<sub>4</sub>)<sub>2</sub>, 3.5 mM NaHCO<sub>3</sub>, 3.5 mM Na<sub>2</sub>CO<sub>3</sub>, and 5.56 mM FeCl<sub>3</sub>, at pH 9, 10  $\mu$ g/mL MamC were added. The formation of the nanoparticles occurred in free-drift experiments for 30 days at 25°C and 1 atm total pressure. The precipitates were magnetically concentrated and rinsed with oxygen-free MilliQ water four times. BMNPs were concentrated to 25 mg/mL in HEPES for synthesis 1 and in PBS for synthesis 2 (detailed below).

### OXA-BMNPs Nanoassemblies Formation

Oxaliplatin (OXA) was immobilized on the surface of BMNPs as described in Jabalera et al.<sup>16</sup> A volume of 1 mL OXA suspension (2 mg/mL) and 5 mg of BMNPs were mixed in HEPES buffer (10 mM HEPES pH 7, 150 mM NaCl) and placed for 72 hours in a Mini LabRoller™ Rotator (Labnet).

UV-Vis spectroscopy (BioMate™ 160 Spectrophotometer, Thermo Scientific) was used to indirectly measure the quantity of adsorbed OXA. For these measurements, the OXA-BMNP nanoassemblies were concentrated with a magnet, and the supernatant was removed and stored. They were washed again with HEPES buffer, magnetically concentrated with a magnet and the supernatant harvested, repeating this procedure for at least three times. The OXA concentration in all collected supernatants was determined from UV/VIS measurements ( $\lambda = 240$  nm), using a previously determined calibration curve. The nanoassemblies were washed until no OXA was detected in the supernatant. The concentration of bound OXA was calculated from the initial concentration by subtracting the released OXA measured in all supernatants collected during the washing protocol.

### Magnetoliposomes Transporting OXA and 5-FU

#### Preparation of Anti-LGR5 Micelles

LGR5 (634J2E) sc-517,661 mouse monoclonal IgG (anti-LGR5) was purchased from Santa Cruz Biotechnology. To remove traces of sodium azide from the stock, it was washed with phosphate-buffered saline pH 7.4 (PBS) and concentrated using 30K Amicon Ultra-0.5 Centrifugal Filter Devices (Millipore). The final concentration of anti-LGR5 was 100  $\mu$ g/mL.

To prepare the micelles, 5 mL of chloroform was used to dissolve 0.5 mg of 1,2-distearoyl-sn-glycero-3-phosphoethanolamine-N-[methoxy(polyethylene glycol)-2000] (18:0 PEG2000 PE, Avanti Polar Lipids) and 44  $\mu$ g of 1,2-distearoyl-sn-glycero-3-phosphoethanolamine-N-[carboxy(polyethylene glycol)-2000] (DSPE-PEG(2000) Carboxylic Acid, Avanti Polar Lipids). Then, vacuum rotatory evaporation was used to remove chloroform. The thin lipid film was hydrated with 0.5 mL PBS and sonicated for 3 minutes at 55°C using an EMMI®-30HC Ultrasonic cleaner (180 W, 220–240 V, 50–60 Hz, EMAG Germany). Then, the sample was concentrated to 50  $\mu$ L using 30K Amicon Ultra-0.5 Centrifugal Filter Devices (Millipore) and incubated for 30 min with 0.5 mL of 50 mM MES buffer pH 5.5, 0.7 M N-hydroxysuccinimide (NHS) and 0.1 M 1-ethyl-3-(3-dimethylaminopropyl) carbodiimide (EDC). Afterwards, the sample was concentrated again to a volume of 50  $\mu$ L, mixed with 25  $\mu$ g of anti-LGR5, and incubated overnight in PBS (0.5 mL final volume). During this time, a covalent bond was formed between the lipids' carboxylic acids and the antibodies' amine groups. After the incubation, 20 mg/mL glycine was added to the micelles containing anti-LGR5, which were then agitated for 30 min and concentrated to a final volume of 100  $\mu$ L.

## Preparation of the Nanoformulations

PEGylated magnetoliposomes were synthesized as described in Garcia-Pinel et al.<sup>17</sup> All the nanoformulations synthesized in this study are represented in Table 1. Synthesis 1 was performed to encapsulate the nanoassembly OXA-BMNPs, while synthesis 2 encapsulated free 5-FU and free BMNPs, since the efficiency of binding of 5-FU to BMNP was very low.

For synthesis 1, a sample of 2.5 mg of egg L- $\alpha$ -phosphatidylcholine (Egg PC, Avanti Polar Lipids) and 0.5 mg of 1,2-distearoyl-sn-glycero-3-phosphoethanolamine-N-[methoxy(polyethylene glycol)-2000] (18:0 PEG2000 PE, Avanti Polar Lipids) were dissolved in 5 mL chloroform. For the nanoformulations containing DiO (Table 1), 62.5  $\mu$ L of a chloroform solution of DiO (10 mg/mL) were also added. Once the lipids were mixed, vacuum rotatory evaporation was used to remove the chloroform, and the film was subsequently hydrated with 0.4 mL BMNPs (25 mg/mL; samples BML1, BML1-DiO, BML1-LGR5, and BML1-LGR5-DiO) or OXA-BMNPs (25 mg/mL of BMNP in the nanoassembly; samples BML1-OXA and BML1-OXA-LGR5) in HEPES buffer. All the samples were agitated at 37°C for 30 min (200 rpm) and sonicated for 5 min at 45°C. A volume of 100  $\mu$ L of anti-LGR5 micelles was added to those nanoformulations anti-LGR5-bearing, and 100  $\mu$ L of HEPES buffer were added to the rest. Finally, the samples were sonicated at 45°C for 5 min and stored at 4°C. To ensure that no OXA was released during the encapsulation in the liposome, the concentration of encapsulated OXA in BML1-OXA and BML1-OXA-LGR5 was indirectly determined from UV-VIS measurements of the OXA in the supernatant harvested after successive washing on these nanoformulations, following the protocol described above.

For synthesis 2, the protocol was identical as above with small variations, since in this case, the system to be encapsulated together was free BMNPs and free 5-FU. These modifications to the protocol of synthesis 1 were: 1) firstly, 10 mg BMNPs were washed five times with chloroform and mixed with the lipids, previously to the vacuum rotatory evaporation; 2) the films were hydrated either with PBS and the BMNP suspension detailed above (samples BML2, BML2-DiO, BML2-LGR5, and BML2-LGR5-DiO) or 2 mg/mL 5-FU in PBS along with the BMNP suspension (BML2-5-FU and BML2-5-FU-LGR5). The concentration of encapsulated 5-FU was determined by following the same protocol as that used for OXA but using the relevant calibration curve for 5-FU previously determined.

## Characterization of BMNPs

Transmission electron microscopy (TEM, Libra 120 PLUS microscope, Carl Zeiss SMT) was used to determine the morphology and size of BMNPs on ultrathin sections, prepared as described in Garcia-Rubia et al. The crystal size was measured on 1000 nanoparticles per experiment using ImageJ 1.47. The solid mineralogy was determined by powder X-ray diffraction (XRD, Xpert Pro X-ray diffractometer, PANalytical; The Netherlands; Cu K $\alpha$ , 20–60° in 2 $\theta$ , 0.01°/step, 3 s per step). Identification of the precipitates was performed by using X Powder software.<sup>26</sup> Electrophoretic mobility

**Table 1** Synthesized Nanoformulations

Abbreviation	Composition
BML1	PEgylated magnetoliposome containing BMNPs (synthesis 1)
BML1-DiO	PEgylated magnetoliposome labeled with DiO containing BMNPs (synthesis 1)
BML1-OXA	PEgylated magnetoliposome containing BMNPs loaded with OXA (synthesis 1)
BML1-LGR5	LGR5-targeted pegylated magnetoliposome containing BMNPs (synthesis 1)
BML1-LGR5-DiO	LGR5-targeted pegylated magnetoliposome labeled with DiO containing BMNPs (synthesis 1)
BML1-OXA-LGR5	LGR5-targeted pegylated magnetoliposome containing BMNPs loaded with OXA (synthesis 1)
BML2	PEgylated magnetoliposome containing BMNPs (synthesis 2)
BML2-DiO	PEgylated magnetoliposome labeled with DiO containing BMNPs (synthesis 2)
BML2-5-FU	PEgylated magnetoliposome containing BMNPs and 5-FU (synthesis 2)
BML2-LGR5	LGR5-targeted pegylated magnetoliposome containing BMNPs (synthesis 2)
BML2-LGR5-DiO	LGR5-targeted pegylated magnetoliposome labeled with DiO containing BMNPs (synthesis 2)
BML2-5-FU-LGR5	LGR5-targeted pegylated magnetoliposome containing BMNPs and 5-FU (synthesis 2)

measurements (Zetasizer Nano-ZS (Malvern Instruments, Malvern, UK)) were used to calculate  $\zeta$ -potential (Zetasizer software), and the IEP was determined from them (nine replica), as described in García Rubia et al.<sup>10</sup> Briefly, the pH of BMNP suspension in oxygen-free NaClO<sub>4</sub> 10 mM was adjusted to different pH values ranging from 2 to 11 and sonicated for 2 min prior to the measurements.

## Characterization of the Nanoformulations

Transmission electron microscopy (TEM; LIBRA 120 PLUS Carl Zeiss SMT, Germany) was used to observe empty and loaded magnetoliposomes. The samples were magnetically concentrated, and a few microliters were deposited on copper grids with formvar film and stained using negative staining. The hydrodynamic size and electrophoretic mobility (and  $\zeta$ -potential) at pH 7.4 were measured (or calculated) as detailed above.

## Nanoformulations as Magnetic Hyperthermia Agents

To determine the magnetic properties and the ability to generate hyperthermia of the nanoformulations, the specific absorption rate (SAR) was calculated. The temperature rise was measured with D5 Series (nB nanoScale Biomagnetics) with a fiber optic sensor. Nanoformulations with a concentration of 0.5 mg/mL Fe contained in a 1 mL aqueous solution were subjected to an alternating magnetic field (MHT) at 385 kHz frequency and 28 kA/m magnetic field for 25 min. The SAR value (W/g) was calculated using the following formula:<sup>27</sup>

$$\text{SAR} = (C_p \text{H}_2\text{O} \times m_{\text{H}_2\text{O}} / m_{\text{BMLs}}) \times (dT/dt) [\text{kWg}_{\text{Fe}}^{-1}]$$

where  $C_p \text{H}_2\text{O}$  was the specific heat of water (J/g K),  $m_{\text{H}_2\text{O}}$  was the mass of water (g),  $m_{\text{BMLs}}$  was the mass of Fe (g) present in BMLs and  $(dT/dt)$  was the slope of temperature rise within the first 1500 s of the heating curve.

## Cell Culture

The human colon cancer cell lines RKO, SW480, HT29, T84, HCT116, HCT15, and the hepatocellular cell line HepG2 were obtained from the American Type Culture Collection (Rockville, MD, USA). The murine cell line MC38 of colon adenocarcinoma was kindly provided by Dr. J. Scholl (Public Health Service, National Institutes of Health, Bethesda, MD, USA). Cells were maintained in Dulbecco's Modified Eagle's Medium (DMEM), which were complemented with penicillin-streptomycin (1%), and fetal bovine serum (FBS) (10%) (Sigma-Aldrich, Madrid, Spain). All the cell lines were cultured at 37 °C and 5% CO<sub>2</sub>.

## Cellular Transduction

LGR5 shRNA (m) lentiviral particles (sc-62,560-V, Santa Cruz Biotechnology, Dallas, Texas, EEUU) were used to inhibit LGR5 gene expression in the mouse colon cancer cell line MC38 following the manufacturer's protocol. 6-well plates were used to seed MC38 cells at the density required to achieve 50% confluence on the day of viral infection. After 24 hours of incubation, media was changed with a mixture of DMEM and 5  $\mu\text{g/mL}$  Polybrene (sc-134,220, Santa Cruz Biotechnology, Dallas, Texas, EEUU). Then, LGR5 shRNA (m) and control shRNA lentiviral particles-A (sc-108,080, Santa Cruz Biotechnology, Dallas, Texas, EEUU) were thawed and added to the culture to infect cells. The cells were incubated for 24 hours and afterwards, the medium was changed with supplemented DMEM. Selection of transduced cells was carried out through exposition to puromycin dihydrochloride at 4  $\mu\text{g/mL}$  (sc-108,071, Santa Cruz Biotechnology, Dallas, Texas, EEUU) and MC38-L(-) (LGR5 negative), and control shRNA cell lines were generated.

## Real Time PCR

The extraction of total RNA was performed with the RNeasy Mini Kit (Qiagen, MD, USA), and the quantity of RNA obtained was quantified with NanoDrop 2000 (Thermo Fisher, Waltham, MA, USA). The retrotranscription to cDNA was carried out with the retro-transcriptase kit (Promega, Madison, WI, USA), in which 1.5  $\mu\text{g}$  of RNA were converted into cDNA according to manufacturer's protocol. SYBR green supermix (Taq Universal SYBR Green Supermix) (Bio-Rad Laboratories, Hercules, CA, USA) was used to perform Real-Time PCR (RT-PCR). The analyzed gene was LGR5 from mouse and human and Glyceraldehyde-3-phosphate dehydrogenase (GAPDH) was used as reference gene (Table S1).

StepOnePlus Real-Time PCR system (Thermo Fisher Scientific, Waltham, MA, USA) was used to perform all quantitative RT-PCR by the delta-delta Ct ( $2^{-\Delta\Delta Ct}$ ) method to obtain gene relative expression values.

## Western Blot Analysis

RIPA (Radio-Immunoprecipitation Assay) lysis buffer (Thermo Fisher Scientific, Waltham, MA, USA) was used to extract proteins from cells, and protein concentration was established by Bradford method (Sigma–Aldrich, Madrid, Spain). Separation of proteins was carried out in 8% SDS-PAGE gels in which 40  $\mu$ g of proteins of each sample were loaded previously heated at 65 °C for 20 minutes. Then, proteins were electrotransferred to a nitrocellulose membrane (45  $\mu$ m pore size) (Millipore, Burlington, MA, USA) and blocked for 1 hour in 5% milk in TBS with 0.1% Tween-20 (TBS-T) (Bio-Rad, Hercules, CA, USA). After several washes in TBS-T, the incubation of the anti-LGR5 primary antibody (1:750) (Anti-LGR5 (OTI2A2): MA5-25,644; Invitrogen, Waltham, Massachusetts, USA) was performed overnight at 4 °C. Then, a secondary antibody (m-IgGkBP-HRP: sc-516,102; Santa Cruz Biotechnology, Dallas, Texas, EEUU) was added (1:2000) for 1 hour at room temperature. Chemiluminescent reagents (Amersham Biosciences, Saint Louis, MO, USA) were used for the detection of membrane-bound antibodies. Besides, anti- $\beta$ -actin IgG (A3854, Sigma Aldrich, Madrid, Spain) (1:25,000 dilution) was used as an endogenous control. The open-source Fiji image analysis software was used to quantify the bands obtained to calculate relative protein expression.<sup>28</sup>

## Cell Proliferation Assays

Forty-eight-well plates were used to culture cells at different densities ( $5 \times 10^3$  cells/well for T84, SW480, HCT15, and RKO;  $1.5 \times 10^4$  cells/well for HT29;  $7 \times 10^3$  cells/well for HCT116;  $2.5 \times 10^3$  cells/well for MC38;  $3 \times 10^3$  cells/well for MC38-L(-); and  $5 \times 10^4$  cells/well for HepG2). After overnight incubation, cells were treated with increasing concentrations of BML1-OXA, BML2-5-FU, BML1-OXA-LGR5, BML2-5-FU-LGR5, OXA, 5-FU, and blank nanoformulations BML1 and 2 were for 4, 8 or 72 hours. The percentage of proliferation was established by the Sulforhodamine B (SRB) assay by measuring the samples at 492 nm (Titertek multiscan Colorimeter, Flow, Irvine, CA, USA), as described previously.<sup>29</sup> The analysis of proliferation in short exposure times experiments was realized by 3-(4,5-Dimethylthiazol-2-yl)-2,5-Diphenyltetrazolium Bromide (MTT) (Sigma–Aldrich, Madrid, Spain) protocol (Cabeza et al, 2021). Relative proliferation (RP) was calculated as a percentage as follows:

$$RP = (\text{treatment absorbance}/\text{untreated control absorbance}) \times 100$$

For the in vitro evaluation of magnetic hyperthermia 8-well chamber slides were used to seed  $5 \times 10^3$  HCT116 cells/well, and after attachment to surface were treated with BML1 and BML2 for 6 hours. After that, cells were subjected for 90 min to a magnetic field within allowed clinical ranges (262 kHz; 17 kA/m) and incubated for 4 hours at 37 °C. After washing, new DMEM was added and incubated for an additional 72 hours. Finally, cell proliferation was analyzed with the Cell Counting Kit-8 (CCK-8) (Dojindo Laboratories, Kumamoto, Japan) at 450 nm of absorbance (Titertek multiscan Colorimeter, Flow, Irvine, CA, USA), and the percentage of relative proliferation was obtained following the above equation.

## Cell Internalization of BMLs and BMLs-LGR5

### Prussian Blue Iron Stain

Twelve-well plates were used to seed T84 and SW480 CRC cells at a density of  $2 \times 10^5$  cells/well. After cells were attached to plate surface, blank BMLs and BMLs-LGR5 were added (iron concentration ranging from 10 to 100  $\mu$ g/mL) for 24 hours. Then, for iron staining Prussian blue technique was used as described previously.<sup>17</sup> Briefly, after cell fixation with 4% formaldehyde, they were incubated with 20% hydrochloric acid and 10% potassium ferrocyanide trihydrate (v/v) for 30 min. After that, cell nuclei were stained with Nuclear Fast Red solution (Sigma-Aldrich) for 15 min. Samples were then observed by light microscopy (Leica DM IL LED) (Leica Microsystems S.L.U., Barcelona, Spain).

## Flow Cytometry Analysis

Flow cytometry was used to analyze the cellular uptake of DiO-loaded BMLs1 and 2 magnetoliposomes in cells seeded in 24-well plates ( $1 \times 10^5$  cells/well for T84 and  $8 \times 10^4$  cells/well for MC38 and MC38-L(-)). After cell attachment to plate surface, BML1-DiO, BML1-LGR5-DiO, BML2-DiO, BML2-LGR5-DiO, and free DiO were added to the cultured medium at a final DiO concentration of 5  $\mu\text{M}$  and incubated from 0.5 to 4 hours. Then, cells were detached by trypsinization, and after centrifugation (1500 rpm, 5 min), cell pellets were resuspended in a volume of 200  $\mu\text{L}$  of PBS. Tumor cells were analyzed with BD FACSCanto II flow cytometer (BD BioSciences, San Jose, USA). Flow cytometry data were processed using the FlowJo Software.

## Fluorescence Microscopy

Cell uptake of magnetoliposomes loaded with DiO was also analyzed by fluorescence microscopy (Leica DM IL LED Fluo). Eight-well chamber slides were used to seed T84 ( $2 \times 10^4$  cells/well), MC38, and MC38-L(-) ( $1.5 \times 10^4$  cells/well). After cell attachment to chamber slide surface, they were treated with free DiO and DiO-loaded BMLs1 and 2 at a final DiO concentration of 50  $\mu\text{M}$  for 4 hours. After two washes with PBS, fixation of cells with 4% formaldehyde (20 min) was performed. After 3 washes with PBS, nuclear staining was made with Hoechst 33,258 for 5 minutes (Sigma-Aldrich) (10  $\mu\text{g}/\text{mL}$ ) and the mounting medium Prolong<sup>TM</sup> Gold Antifade Mountant (Invitrogen, Waltham, Massachusetts, USA) and coverslips were added before the observation of the samples under a fluorescence microscope (Leica DM IL LED) (Leica Microsystems S.L.U., Barcelona, Spain).

## In vivo Acute Toxicity Study of BMLs

To determine the in vivo acute toxicity of BMLs, 16 female C57BL/6 mice (6-weeks) were divided arbitrarily into three groups: control ( $n = 4$ ), BML1 ( $n = 6$ ), and BML2 ( $n = 6$ ). A single dose of 45 mg/kg Fe was injected i.v in the tail vein of mice of the BML1 and BML2 groups. The untreated group was inoculated in the same way with saline solution. Mouse body weight was measured every 48 h from the inoculation until day 15. At this point, blood samples were obtained in 1.5 mL EDTA-coated collecting tubes: an aliquot was used to analyze blood populations (Mythic 22CT C2 Hematology Analyzer, Orphée SA, Switzerland), and the rest of the blood was centrifuged to obtain plasma (3000 rpm for 15 min at 4°C) and analyzed for albumin, creatinine, glutamic-oxaloacetic transaminase (GOT), glutamate pyruvate transaminase (GPT), gamma-glutamyl transferase (GGT), alkaline phosphatase (ALP), direct bilirubin, total bilirubin, total proteins, and urea tests in Luminex 200 TM (Millipore, Darmstadt, Germany). Once the blood was collected, the animals were sacrificed, and the organs were obtained and weighed. After the fixation of organs in 4% paraformaldehyde (PFA), they were embedded in paraffin. Sections of 5  $\mu\text{m}$  were obtained and stained with hematoxylin and eosin or Prussian blue. Sections of tissues were observed in a Leica DM IL LED microscope (Leica Microsystems S.L.U., Barcelona, Spain).

## Statistical Analysis

Student's *t*-test, one-way repeated measures ANOVA, and U Mann–Whitney were used to analyze differences between groups with a significance level of 0.05 ( $\alpha=0.05$ ) with the Statistical Package for the Social Sciences (SPSS) (v.28) (IBM Corporation, Armonk, NY, USA). All the results were expressed as the mean  $\pm$  standard deviation (SD).

## Results

### Characterization of BMNPs

BMNPs are well-defined crystals, according to TEM images, with 2D rectangular and rhomboidal shapes (Figure 2A). BMNP size falls within the range 10–70 nm (Figure 2B), being the average size of  $41 \pm 12$  nm. According to XRD analyses (Figure 2C), BMNPs are magnetite (>95%) with an isoelectric point of 4.4 (Figure 2D), meaning that they are negatively charged at physiological pH value and positively charged at pH values lower than 4.4.

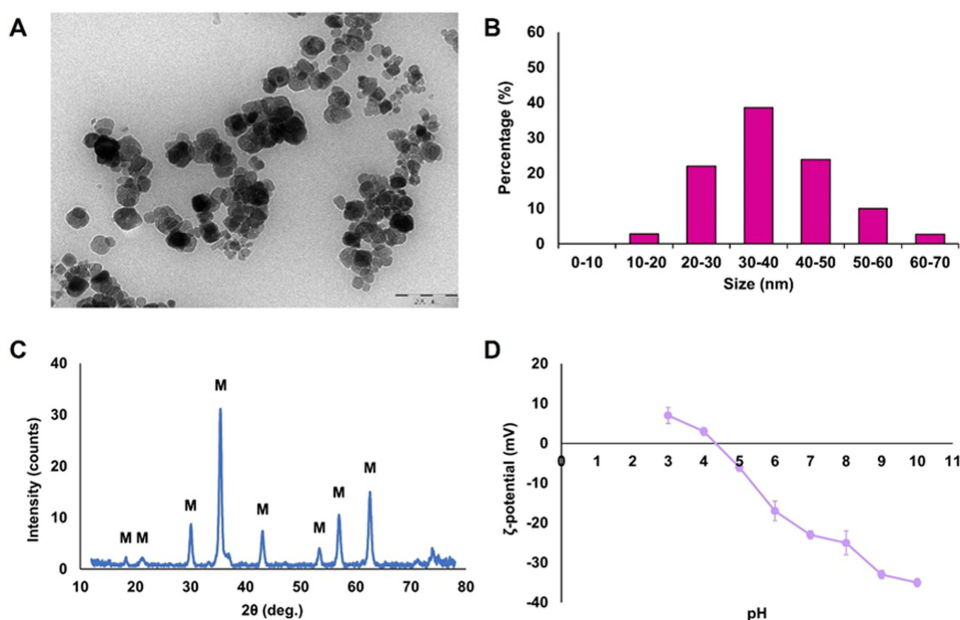


**Figure 2** Characterization of BMNPs. (A) TEM image (scale bar: 200 nm). (B) Size distribution. (C) XRD analysis (M: peaks corresponding to magnetite). (D)  $\zeta$ -potential.

## Synthesis and Characterization of BMLs

The composition of the synthesized nanoformulations is summarized in [Table 1](#). For synthesis 1, the compositions of the nanoformulations were 10 mg/mL BMNPs, 5 mg/mL Egg PC, 1 mg/mL PEG2000 PE, 1.25 mg/mL DiO, 50  $\mu$ g/mL anti-LGR5 and 2 mg/mL OXA (as determined from UV-VIS measurements). For synthesis 2, the compositions of the nanoformulations were 10 mg/mL BMNPs, 5 mg/mL Egg PC, 1 mg/mL PEG2000 PE, 1.25 mg/mL DiO, 50  $\mu$ g/mL anti-LGR5 and 2 mg/mL 5-FU.

TEM images show that magnetoliposomes are composed of lipid bilayers entrapping several BMNPs ([Figure 3A](#)). Most of the BMLs show a hydrodynamic diameter of  $100 \pm 40$  nm ([Figure 3B](#)). There is no difference in size between the blank or loaded BMLs. Regarding the  $\zeta$ -potential, all samples are negatively charged at pH 7.4 ([Figure 3C](#)), which might facilitate the colloidal stability of the suspensions employing electrostatic repulsion among them.<sup>17</sup>

The ability to generate hyperthermia after the application of a high-frequency alternating magnetic field ([Figure 4A](#)) and effect on cell viability was analyzed ([Figure 4B](#)). [Figure 4A](#) shows the heating curves obtained after 25 min of application. All samples were able to increase the temperature to a total  $\Delta T$  of 3.8, 5.1, 7.0, and 6.8  $^{\circ}$ C for BML1, BML1-LGR5, BML2 and BML2-LGR5, resulting in SAR values of 20.9, 28.5, 39.6, and 38.5 W/g, respectively.

## LGR5 Expression Analysis

The study of LGR5 mRNA and protein expression was performed in CRC cell lines from human (RKO, HT29, T84, HCT116, SW480, and HCT15), mouse (MC38 and MC38-L(-)), and the hepatocarcinoma cell line HepG2 ([Figure 5](#)). The cell line HepG2, together with HT29, exhibited the highest level of LGR5 mRNA expression, whereas the SW480 cell line showed the lowest expression ([Figure 5A](#)). Protein expression results of LGR5 obtained by Western blot revealed high levels of LGR5 protein in HCT15 and HepG2 cell lines compared to T84 (increment of 3.3 and 2.6-fold, respectively) ([Figure 5C](#)). A mRNA and protein expression decrease (6- and 2-fold, respectively) was also observed in the transduced cell line MC38-L(-) ([Figure 5B and D](#)).

## In vitro Proliferation Assays

The in vitro antiproliferative effect of free drugs, drug-loaded magnetoliposomes, and blank magnetoliposomes was determined by the SRB assay. No significant differences were observed compared to the negative control in most of

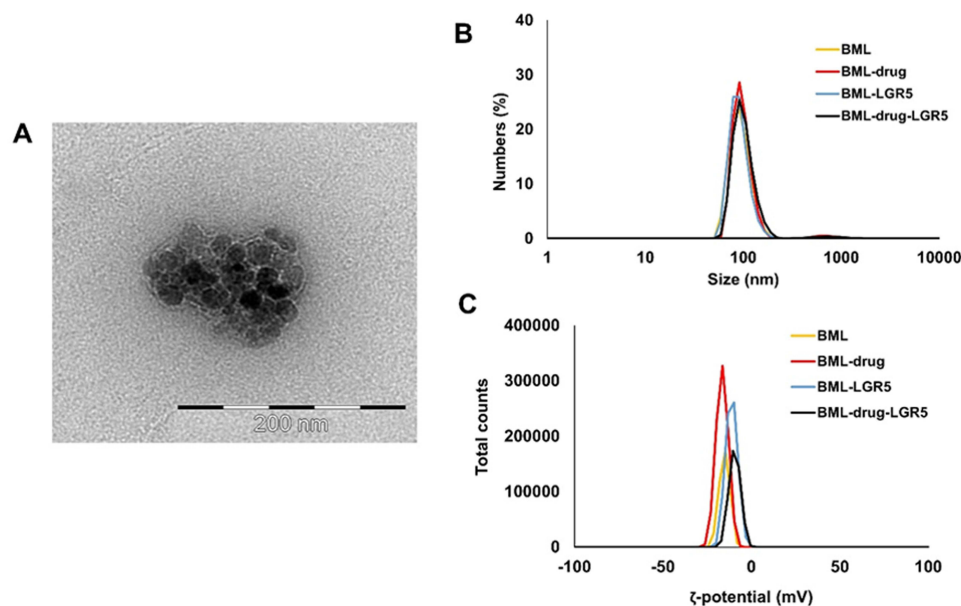


**Figure 3** Characterization of magnetoliposomes. (A) TEM image of BML1. (B) Size distribution. (C)  $\zeta$ -potential. BML-drug and BML-drug-LGR5 refer to those magnetoliposomes loaded either with OXA or with 5-FU.

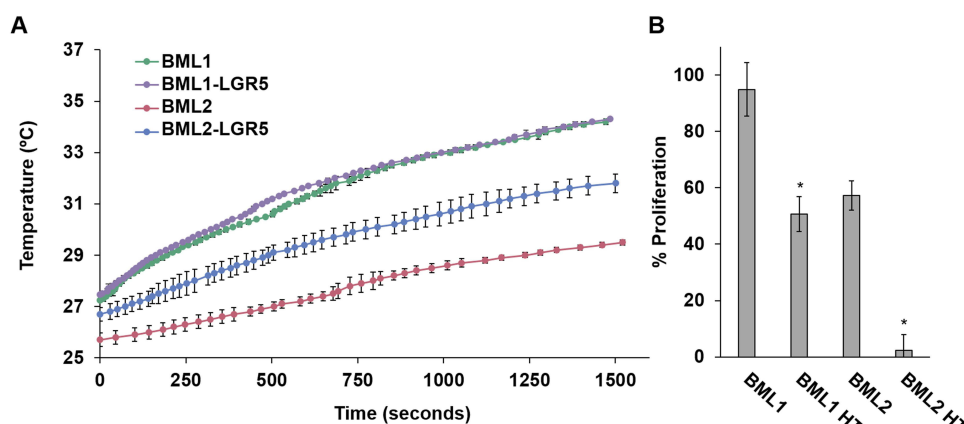


**Figure 4** Magnetic hyperthermia properties of BMLs. (A) Temperature rise after application of an alternating magnetic field (385 kHz; 28 kA/m) during 25 min for BML1, BML1-LGR5, BML2, and BML2-LGR5 at a concentration of 0.5 mg/mL Fe. The data were represented as the mean of 3 measurements  $\pm$  standard deviation (SD). (B) In vitro proliferation assay of HCT116 CRC cells treated with BML1 and BML2 after 72 hours from alternating magnetic field (AMF) application for 90 min. Graphs show the percentage of proliferation of HCT116 at 0.5 mg/mL of Fe. Results were expressed as mean  $\pm$  SD of triplicate cultures. \*P-value < 0.05 compared to BML1 and BML2 and determined by Student's t-test.

the doses tested in cells treated with drug-unloaded magnetoliposomes [BML1 and 2 (LGR5-targeted and non-targeted)] with percentages of relative proliferation higher than 90% (Figures S1–S3). BML1-LGR5 did not show reduced biocompatibility, except in RKO and MC38-L(-) cells at the highest dose (75.0% and 80.4% relative proliferation, respectively).

In the case of drug-loaded nanoformulations, all treatments reduced cell viability in a dose-dependent manner after 72 hours, decreasing or maintaining the  $IC_{50}$  value of free drugs (Figures 6 and 7, Table 2). In fact, the RKO cell line treated with BML1-OXA-LGR5 (72 hours) showed the highest viability reduction in relation to BML1-OXA and OXA  $IC_{50}$  (1.7 and 3.2-folds, respectively ( $p < 0.05$ )), followed by HCT116 (1.5 and 2.5-folds, respectively). On the other hand, BML2-5-FU-LGR5 reduced 5-FU  $IC_{50}$  by more than half in the MC38 and HCT15 cell lines (3.0 and 2.5-folds, respectively) ( $p < 0.05$ ). The trend was similar in the rest of the cell lines with the exception of HT29 and HepG2 treated with BML1-OXA-LGR5, which showed similar viability compared to the free drug treatment. Interestingly, assays using LGR5-

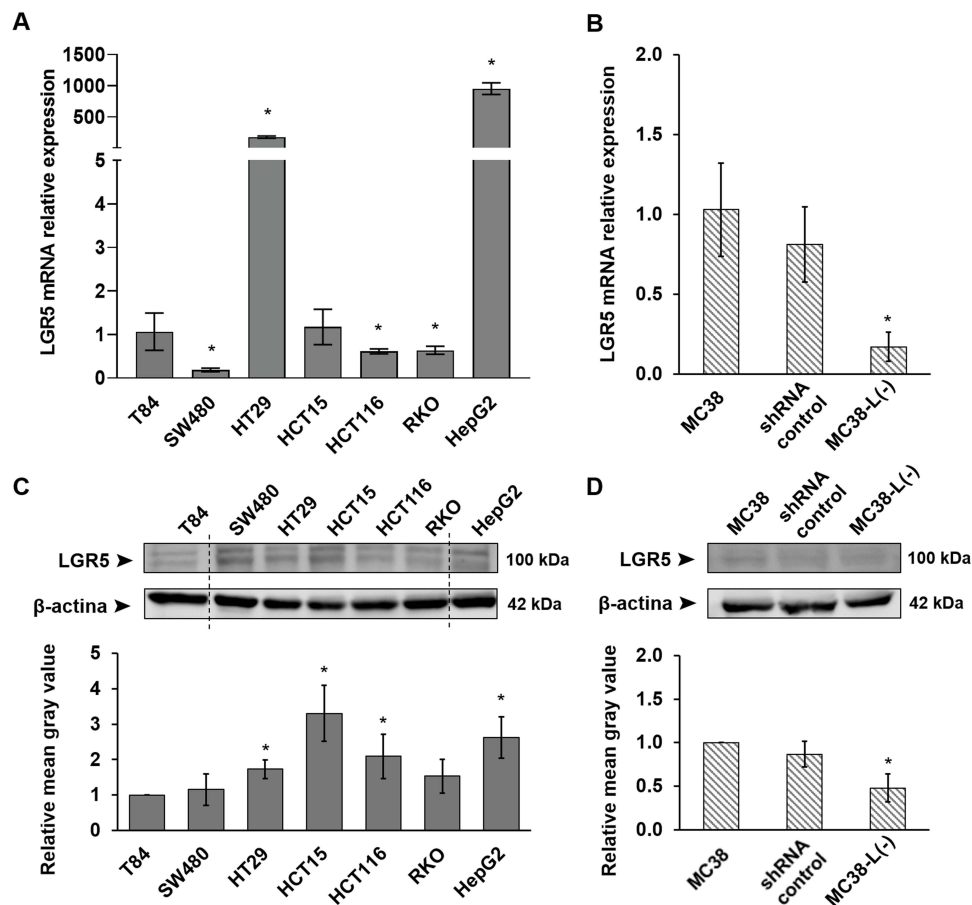


**Figure 5** LGR5 expression analysis in colorectal tumor and hepatocarcinoma cell lines. Relative expression of LGR5 mRNA by Real-time PCR in (A) human and (B) mouse cells compared to T84 and MC38 respectively. Representative Western blot images of LGR5 and  $\beta$ -actin proteins and graphs of bands densitometry analysis in (C) human and (D) murine cells compared to T84 and MC38 respectively. All the results were represented as the mean  $\pm$  SD ( $n=3$ ). \*P-value < 0.05 compared to T84 and MC38 cells and determined by Student's *t*-test.

functionalized BMLs1 at short exposure times (4 and 8 hours) showed higher proliferation inhibition in T84, MC38 and HepG2 cells than non-functionalized BMLs1 and free OXA. The reduction in cell proliferation compared to free 5-FU was maintained in T84, MC38, MC38-L(-), and HepG2 treated with higher doses and short exposure times of nanoformulations (Figure 8).

Cell proliferation of MC38 cells treated with LGR5-bearing and non-bearing nanoformulations showed significant differences (5 and 10  $\mu$ M) ( $p < 0.05$ ). By contrast, no differences were found in MC38-L(-) transduced cell line. Moreover, at short exposition times (4 and 8 hours), cell death was higher with both LGR5-functionalized BMLs compared to that non-functionalized BMLs1 and free drugs (Figure 8). Similar percentages of relative proliferation were observed in the MC38-L(-) transduced cell line treated with drug-loaded BML-LGR5 compared to untargeted drug-loaded BMLs.

Finally, after 90 min of exposure to an alternating magnetic field (AMF) (262 kHz; 17 kA/m) on HCT116 cells previously treated with BML1 and BML2 (0.5 mg/mL Fe; 72 hours) a high decrease in cell viability was observed compared with cells no exposed to AMF (44.2% and 55.3%, respectively). Nevertheless, BML2 appears to be toxic at the iron concentration of 0.5 mg/mL (53.29% relative proliferation) unlike to BML1 (57.3% and 94.9% relative proliferation, respectively) (Figure 4B).

## Cell Internalization of BMLs and BMLs-LGR5

The cell uptake of blank (drug-free) BMLs with and without LGR5 functionalization was analyzed with Prussian blue iron staining. A dose-dependent staining was observed. BML1 and BML2, with and without LGR5 targeting, were

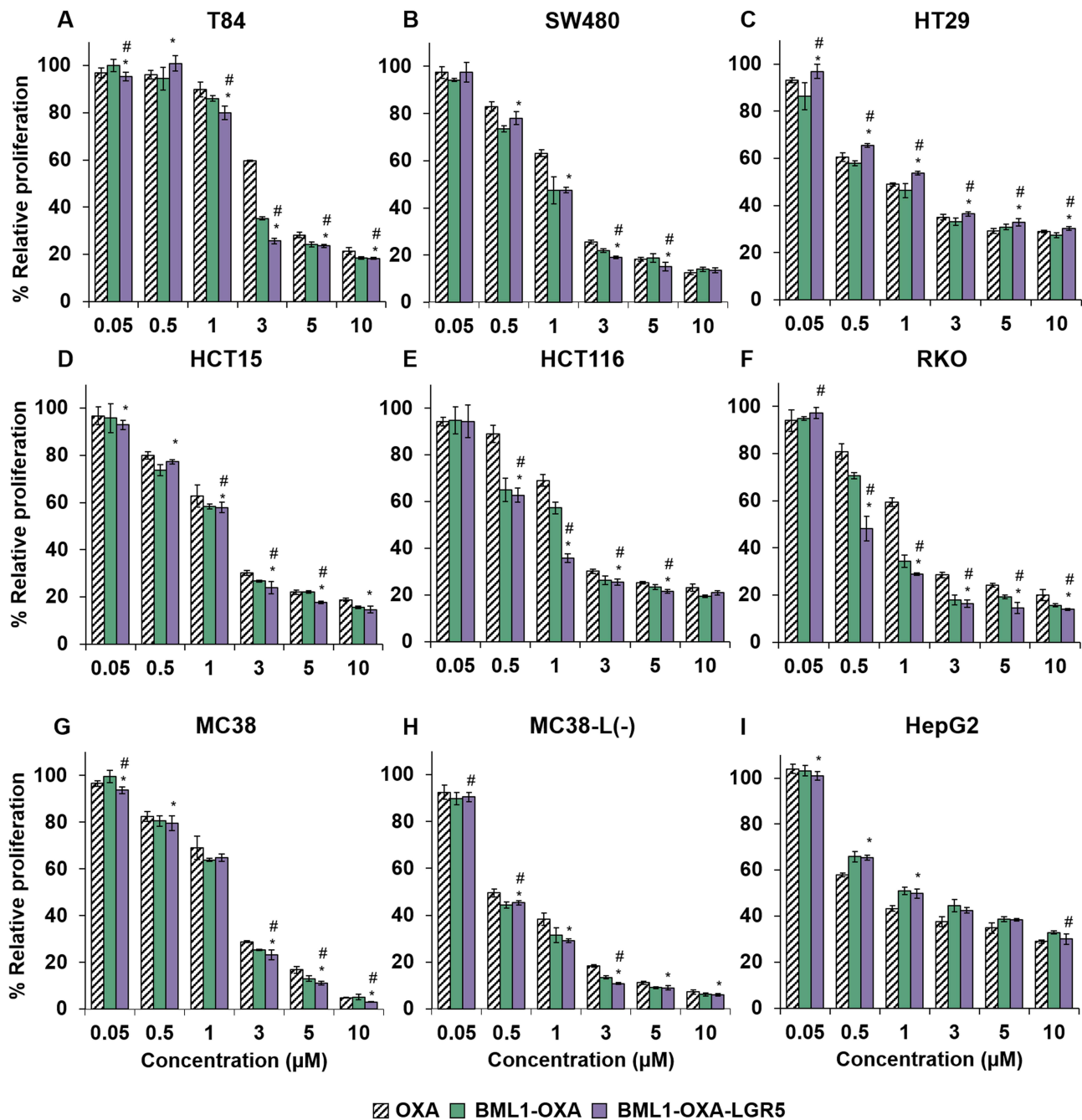


**Figure 6** In vitro cell viability assay of OXA-loaded BML1 with and without LGR5 functionalization. Graphs show the percentage of relative proliferation of (A) T84, (B) SW480, (C) HT29, (D) HCT15, (E) HCT116 (F) RKO, (G) MC38, (H) MC38-L(-) and (I) HepG2 at doses ranging from 0.05–10 μM of OXA after at 72 hours of exposure. Results were expressed as mean ± SD of triplicate cultures. \*<sup>#</sup>P-value < 0.05 compared to OXA and BML1-OXA respectively and determined by Student's t-test.

internalized satisfactorily by tumor cell lines at the time tested (Figures 9 and S4). Furthermore, the T84 cell line appears to be able to internalize slightly more BML1-LGR5 compared to non-targeted BML1 while no apparent differences were observed in BML2 with and without functionalization treatment. However, BML2-LGR5 showed higher cellular uptake in the SW480 cell line compared to BML2.

The cell uptake of DiO-loaded BML1 and BML2 was time dependent and increased with LGR5-targeted magnetoliposomes in all cell lines (Figures 10 and 11). Significant higher internalization of LGR5-BMLs was observed even within the first half an hour of treatment (for T84) and improved after 4 hours of exposure, with increments in cell uptake of 4.5, 1.8, and 1.5-folds for BML1-LGR5-DiO and 2.9, 2.2, and 1.6-folds for BML2-LGR5-DiO in T84,

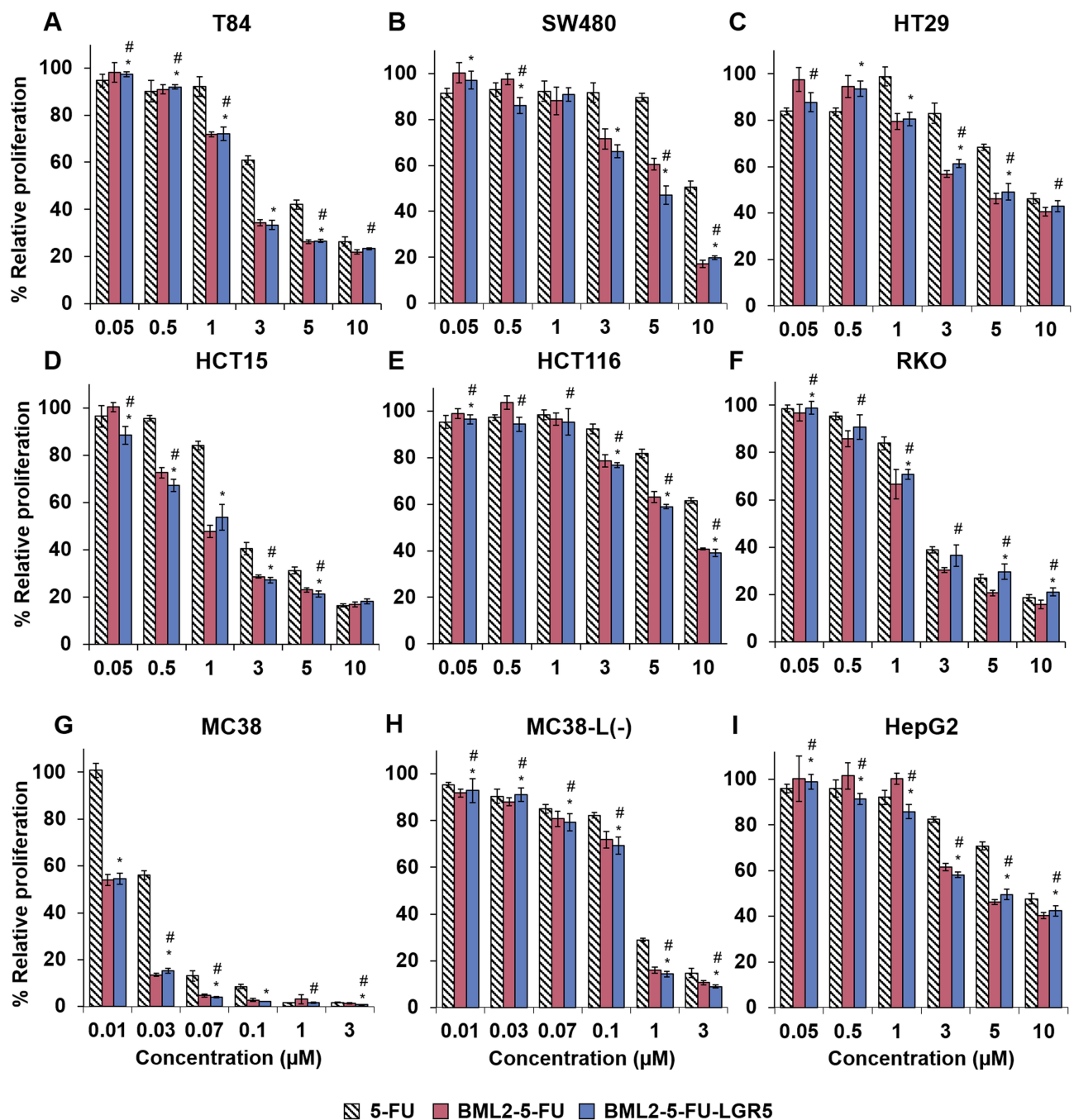


**Figure 7** In vitro cell viability assay of 5-FU loaded BMLs2 with and without LGR5 functionalization. Graphs show the percentage of relative proliferation of (A) T84, (B) SW480, (C) HT29, (D) HCT15, (E) HCT116, (F) RKO, (G) MC38, (H) MC38-L(-) and (I) HepG2 cell lines at doses ranging from 0.01–10 µM of 5-FU after at 72 hours of exposure. Results were expressed as mean  $\pm$  SD of triplicate cultures. \*,#P-value < 0.05 compared to 5-FU and BML2-5-FU respectively and determined by Student's *t*-test.

MC38 and MC38-L(-) cells, respectively, compared to untargeted-BMLs (Figures 10A, 11A and S5–S8). It is noteworthy that the transduced MC38-L(-) cells internalized fewer LGR5-BMLs compared to MC38 (1.9 and 1.5-folds less for BML1 and 2-LGR5-DiO respectively). Slight less internalization of BML1-DiO was also observed in MC38-L(-) cell (1.6-folds).

Microscopy images showed similar results to those obtained in flow cytometry. Due to the lipophilic nature of free DiO, it was only slightly presented in the cell membrane not inside cells, whereas DiO-loaded BMLs were highly internalized by tumor cells observing it in cell cytoplasm with no co-localization with cell nuclei

**Table 2** Half Inhibitory Concentration (IC<sub>50</sub>) of LGR5-Targeted and Non-Targeted BMLs1 and 2 (μM) Treatment (72 Hours) in the Cell Lines Tested

Cell Line	Free drug		Non-Targeted BMLs		LGR5-BMLs		Times that LGR5-BMLs Reduces IC <sub>50</sub> of Free Drug		Times that LGR5-BMLs Reduces IC <sub>50</sub> of Non-Targeted BMLs	
	OXA	5-FU	BML1-OXA	BML2-5-FU	BML1-OXA-LGR5	BML2-5-FU-LGR5	BML1	BML2	BML1	BML2
T84	3.45	4.24	2.42	2.18	2.08	2.20	1.66	1.93	1.16	0.99
SW480	1.52	10.18	1.00	5.29	1.06	4.46	1.43	2.28	0.94	1.19
HT29	1.19	9.43	0.95	4.93	1.50	5.85	0.79	1.61	0.63	0.84
HCT15	1.62	2.69	1.35	1.16	1.31	1.08	1.24	2.49	1.03	1.07
HCT116	1.98	13.51	1.19	7.47	0.79	6.96	2.51	1.94	1.51	1.07
RKO	1.56	2.59	0.82	1.76	0.48	2.29	3.25	1.13	1.71	0.77
MC38	1.63	0.03	1.41	0.01	1.38	0.01	1.18	3.00	1.02	1.00
MC38-L(-)	0.55	0.42	0.42	0.24	0.42	0.22	1.31	1.91	1.00	1.09
HepG2	1.21	9.62	2.08	5.43	1.73	5.59	0.70	1.72	1.20	0.97

(Figures 10B, 10C and 11B, 11C). Cells treated with LGR5-targeted nanoformulations showed higher green fluorescence in their cytoplasm compared with non-targeted formulations, with a punctate pattern in the cytoplasm of cells treated with BML1-DiO with and without LGR5. In addition, the fluorescence intensity of MC38-L(-) treated with BML1 and 2-LGR5-DiO was fewer compared to that of MC38, showing therefore, less nanoformulation cell uptake.

## In vivo Acute Toxicity Study

In vivo biocompatibility of the magnetoliposomes was evaluated in terms of iron-related toxicity. Acute intravenous exposure to BML1 and BML2 showed no signs of toxicity as no mortality was observed, and the overall health of the animals was not affected by any treatment. Furthermore, no relevant body (Figure 12A) or organ weight (Figure 12B) loss over time was detected compared to untreated mice. Only BML2 group did not showed weight gain. In addition, Prussian blue staining revealed the presence of iron in the liver with BML1 and BML2 treatment, but no signs of toxicity in liver tissue structure were observed with hematoxylin and eosin staining (Figure 12C). No iron deposits were found in any organ stained with Prussian blue except in splenic red pulp in all groups of mice including the untreated control. In addition, staining of all organs with hematoxylin and eosin showed no sign of toxicity for any of the treatments (Figures S9 and S10).

Additionally, blood biochemical analysis showed no significant differences of BML1 and BML2 compared to untreated control in all parameters analyzed (Table 3), with the exception of alkaline phosphatase analysis in which lower values were observed with BML2 treatment. In general no significant differences were found in blood population analysis between the mice groups (Table 4) except for increased values of hematocrit and percentage of eosinophils for BML1 and BML2 treatment, decreased white blood cells total number and percentage of monocytes/macrophages for BML1 treatment, and increased hemoglobin, neutrophil/polymorphonuclear percentage and decreased lymphocyte percentage for BML2 treatment ( $p < 0.05$ ).

## Discussion

It is widely known that active targeting approaches are gaining importance in cancer therapy because of the increasing efficiency and specificity of drugs for tumor tissues, reducing side effects. The combination of liposomes and magnetic nanoparticles in a unique nanoformulation named magnetoliposome creates a range of possibilities in the field of drug delivery systems, including controlled release of drugs, hyperthermia, and active targeted drug delivery by surface functionalization of liposomes.<sup>30–32</sup> Besides, functionalization of the nanoformulations is an advantage preventing diffusion of the nanoparticles into the extracellular matrix of the tumor<sup>31</sup> and recognizing specifically tumor cells, internalized by receptor-mediated endocytosis.<sup>31,33,34</sup> In particular, the strategy proposed in our study is the targeting of

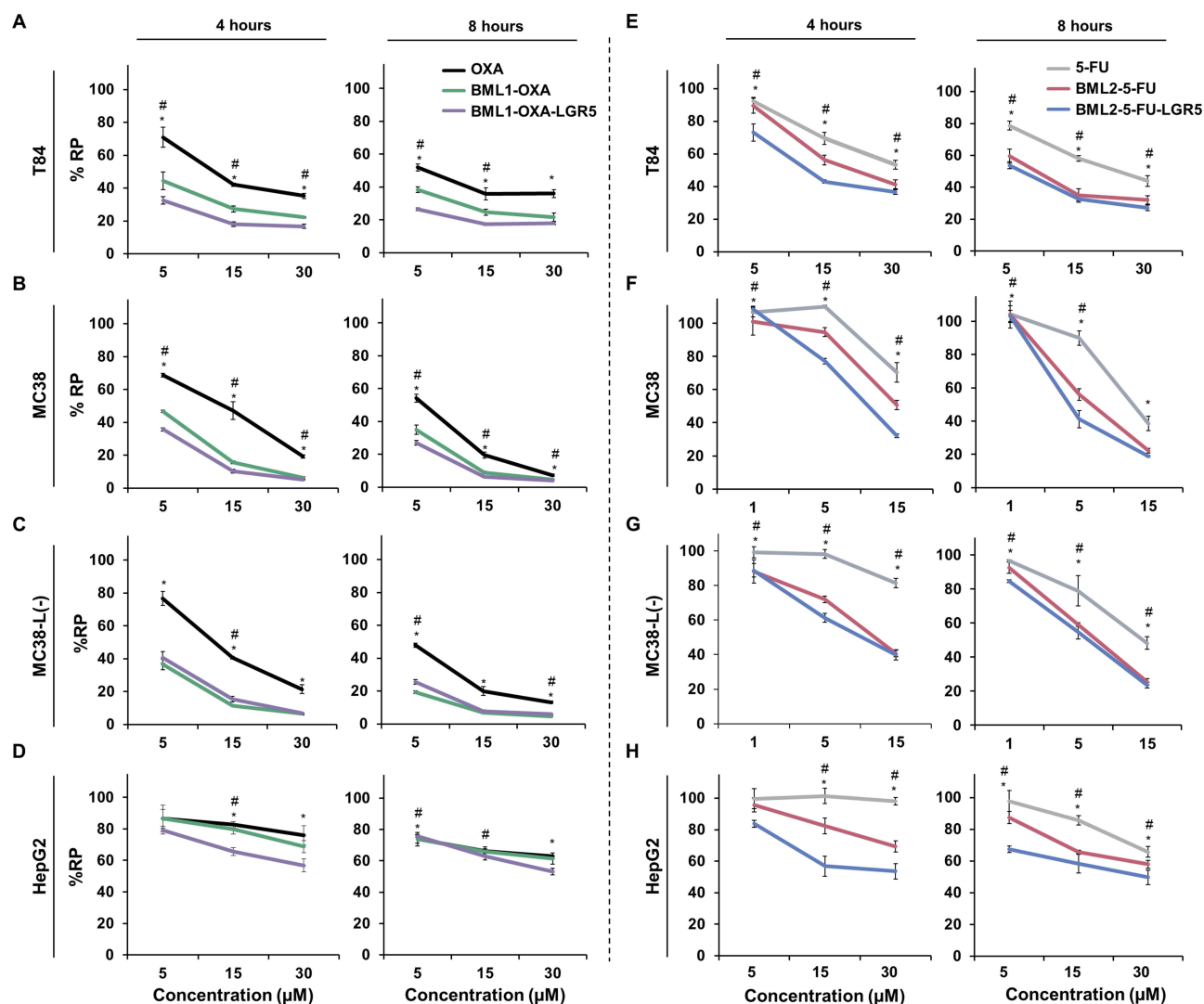


**Figure 8** In vitro proliferation assay of drug-loaded BML1 and 2 with and without LGR5 functionalization at short exposure times. Percentage of relative proliferation (%RP) of (A) T84, (B) MC38, (C) MC38-L(-) and (D) HepG2 treated with doses ranging from 5–30  $\mu\text{M}$  of OXA for 4 and 8 hours. (E) T84, (F) MC38, (G) MC38-L(-) and (H) HepG2 were treated with doses ranging from 1–30  $\mu\text{M}$  of 5-FU for 4 and 8 hours. Results were expressed as mean  $\pm$  SD of triplicate cultures. \*<sup>#</sup>P-value < 0.05 between LGR5-targeted BMLs and free drug or non-targeted BMLs respectively and determined by Student's t-test.

magnetoliposomes loaded with OXA or 5-FU through the surface binding of an anti-LGR5 antibody, a coreceptor of the Wnt/ $\beta$ -catenin signaling pathway.<sup>23,35,36</sup>

As we previously described,<sup>14</sup> OXA binds to BMNPs based on electrostatic interactions at physiological pH values, due to the negative charge of BMNPs at this pH (Figure 2D). According to Figure 2D and in agreement with data in Jabalera et al<sup>14</sup> and Garcia-Pinel et al,<sup>17</sup> this nanoassembly is stable at physiological pH values as BMNPs remain charged. At acidic pH values, BMNPs will become uncharged, as they approach their isoelectric point, thus releasing the drug. Little to no OXA release was detected during the embedding, as the hydration of the lipid layer was performed in HEPES buffer. On the contrary, 5-FU is negatively charged at the functionalization pH value (pH = 7), as it is well known that the pKa of the 5-FU is 8.0.<sup>37</sup> Since at this pH value BMNPs are also negatively charge (Figure 2D), the electrostatic binding does not occur, and so, BML2 embed a suspension of BMNPs in free 5-FU.

Our results showed that magnetoliposome-based nanoformulations that bind anti-LGR5 antibody did not show toxicity. Previously, the biocompatibility of BML1 (non-targeted) was previously reported by Garcia-Pinel et al, in T84, SW480, HT29, HCT15, and MC38 cell lines.<sup>17</sup> Interestingly, after 72 hours of exposure, BML1-OXA-LGR5

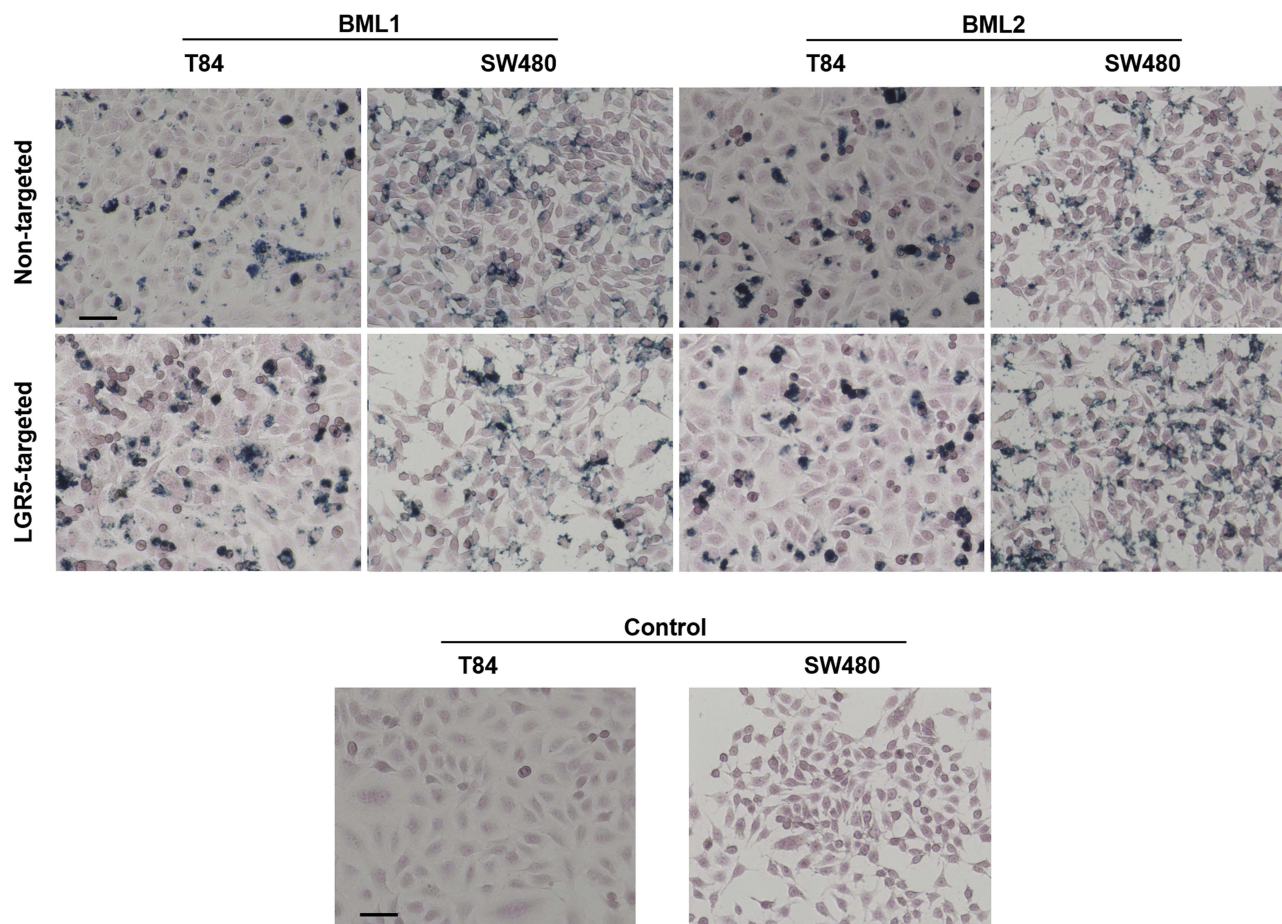


**Figure 9** Internalization of magnetoliposomes with and without LGR5 functionalization in T84 and SW480 cell lines. Representative images of cells exposed (24 hours) to 50  $\mu\text{g/mL}$  Fe of BML1, BML1-LGR5, BML2 and BML2-LGR5 stained with Prussian blue. Scale bar 50  $\mu\text{m}$ .

exhibited enhanced or maintained antitumor activity compared to non-targeted nanoformulation in all cell lines. In addition, this nanoformulation induced a higher cytotoxicity than BML2-5FU-LGR5 despite reduced  $\text{IC}_{50}$  values of free 5-FU in all cell lines studied. Due to the evident internalization of the BMLs from short times,<sup>17</sup> proliferation experiments at this same time were carried out to further demonstrate the advantages of active targeting. Our results showed a significant increase of BML-OXA-LGR5 antitumor effect in MC38 cells after 4 hours of treatment compared to the MC38-L(-) transduced cell line, which was probably due to expression silencing of LGR5 in these latter cells. This improved effect suggests that the enhanced antitumor activity of LGR5-targeted BMLs in MC38 may be related to the specific binding of the nanoformulations to the LGR5 receptor on the cell membrane.<sup>38–40</sup> However, the cause of the increased sensitivity to chemotherapy and the longer doubling time observed in MC38-L(-) compared to the non-transduced cell line is unclear. LGR5 is a membrane receptor involved in the Wnt/ $\beta$ -catenin signalling pathway, so reduction of its expression may lead to changes in the proliferation rate.<sup>41</sup> In addition, magnetoliposome-based nanoformulations were able to modify cell proliferation by magnetic hyperthermia. In fact, HCT116 CRC subjected to AMF have shown a great reduction of cell viability for BML1 and 2 (up to 44.2% and 55.3%, respectively). Hence, these magnetoliposomes could be a good LGR5-targeted chemotherapy treatment option in combination with magnetic hyperthermia in CRC management. The therapeutic benefit of combined chemotherapeutic drugs with magnetic hyperthermia mediated magnetic nanoparticles have been extensively demonstrated<sup>15,42</sup> such as the chemothermal combination of doxorubicin-loaded biomimetic magnetic nanoparticles with an alternating magnetic field significantly reduced the tumor volume in a murine model of breast cancer.<sup>12</sup> Therefore, higher interest is growing related with the

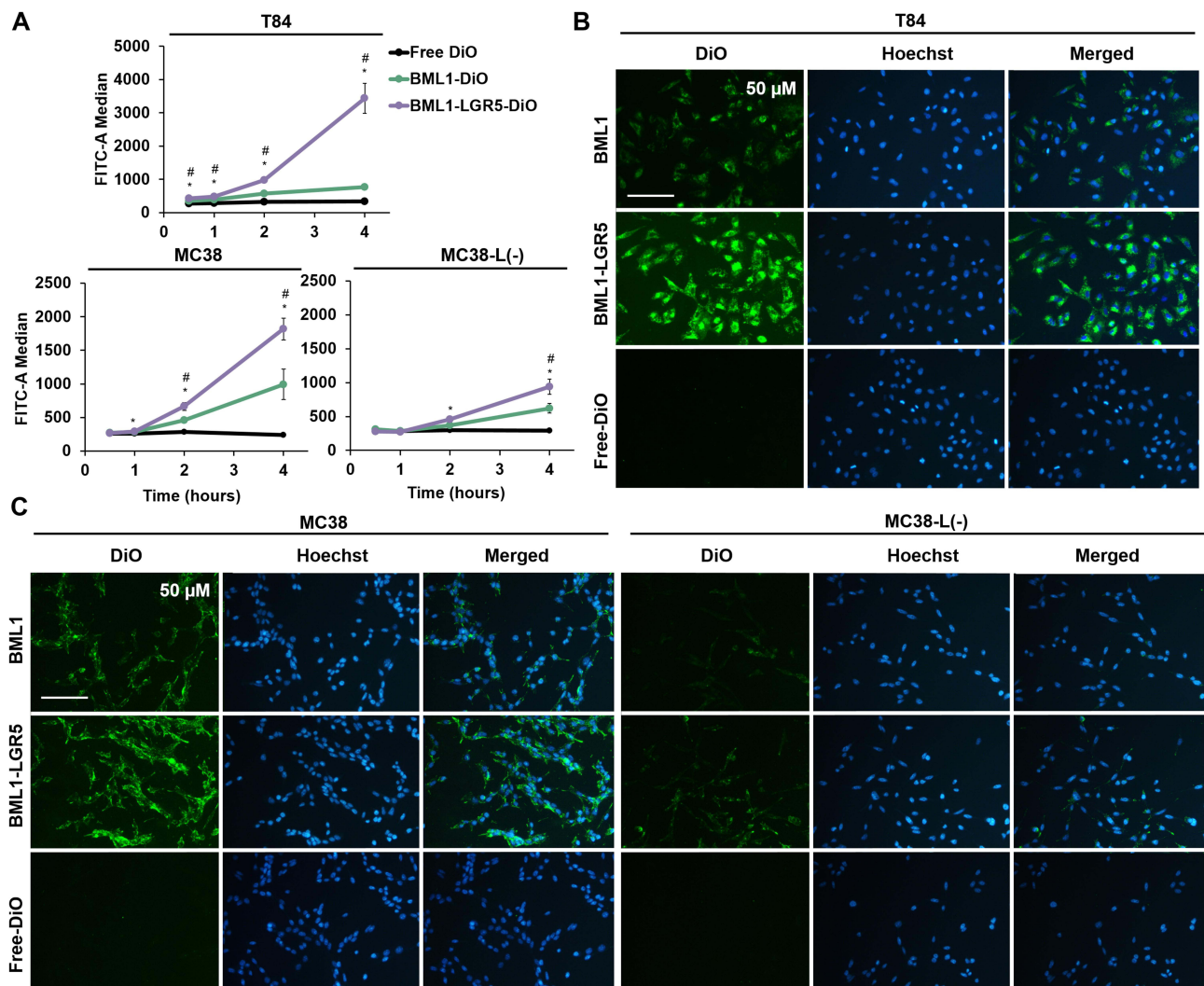


**Figure 10** Cell uptake of LGR5-targeted and untargeted BML1-DiO. **(A)** Quantitative measure of DiO cell uptake by flow cytometry in T84, MC38 and MC38-L(-) cells. Data represent mean  $\pm$  SD of triplicate cultures. (\*, #) P-value < 0.05 compared to free DiO and BML1-DiO respectively and determined by Mann Whitney U-test. **(B and C)** Representative images of fluorescence microscopy analysis of DiO cell uptake in T84, MC38, and MC38-L(-) cells. Hoechst 33,258 which stain cell nuclei was shown as blue, and DiO was shown as green fluorescence. Merge images are showed of DiO and Hoechst 33,258 for the different treatments. Scale bar 100  $\mu$ m.

design of new multifunctional nanoformulations, as active targeted magnetoliposomes among others, which allow combined therapy.

In this context, our results showed that the functionalization of magnetoliposomes with anti-LGR5 antibodies improved cellular uptake compared to untargeted nanoformulations in all the cell lines tested. This fact was confirmed by cell uptake studies of BML nanoformulations including DiO, a green fluorescent lipophilic dye that labels cell membranes and cannot be observed in cell cytoplasm.<sup>43</sup> All the cells treated with these nanoformulations exhibited high green fluorescence in cytoplasm indicating the presence of magnetoliposomes inside cells. It was also possible to quantify these cell internalization levels by flow cytometry. Our results showed that the functionalization of magnetoliposomes with anti-LGR5 antibodies improved cellular uptake compared to untargeted nanoformulations in all the cell lines tested. Specifically, BML1-LGR5 enhanced cellular uptake in T84 and MC38 cells (4.5 and 1.8-fold, respectively) after 4 hours of exposition in comparison to untargeted BMLs. In contrast, the transduced cell line MC38-L(-) showed lower internalization of LGR5-targeted BMLs (synthesis 1 and 2) compared to the MC38 cell line. These differences found between the wild-type MC38 and the transduced MC38-L(-) cell line could be due to the specific internalization of targeted-BMLs by ligand–receptor interaction.<sup>19,39,44</sup> Although the data obtained in

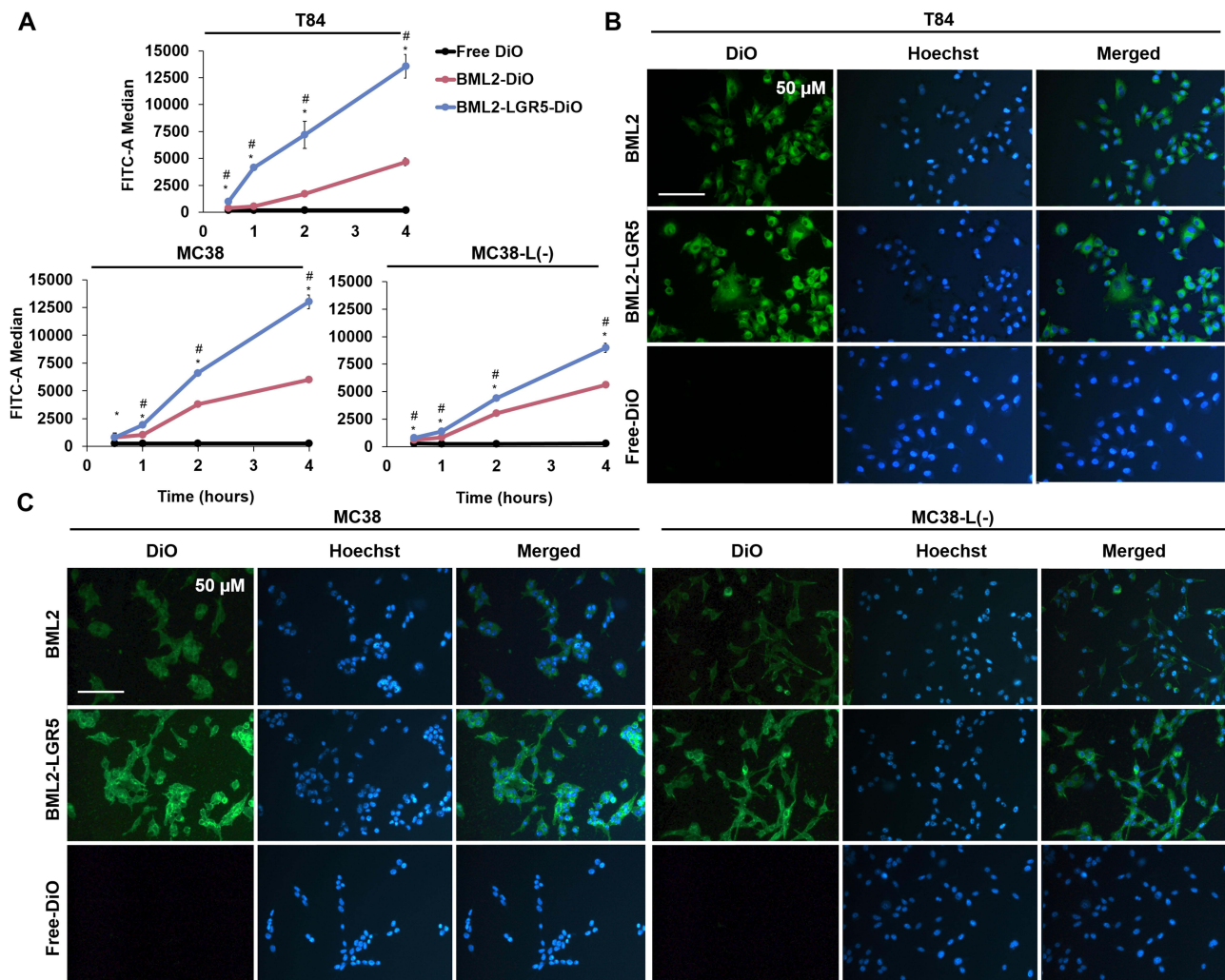


**Figure 11** Cell uptake of LGR5-targeted and untargeted BML2-DiO. **(A)** Quantitative measure of DiO cell uptake by flow cytometry in T84, MC38 and MC38-L(-) cells. Data represent mean  $\pm$  SD of triplicate cultures. \*,#P-value < 0.05 compared to free DiO and BML2-DiO respectively and determined by Mann Whitney U-test. **(B and C)** Representative images of fluorescence microscopy analysis of DiO cell uptake in T84, MC38, and MC38-L(-) cells. Hoechst 33,258 which stain cell nuclei was shown as blue, and DiO was shown as green fluorescence. Merge images are showed of DiO and Hoechst 33,258 for the different treatments. Scale bar 100  $\mu$ m.

cell internalization experiments could suggest a receptor-mediated nanoparticle–cell interaction, other mechanisms of action could be implicated. Different forms of cell–liposome interaction have been described. Thus, liposomes may bind to the plasma membrane by electrostatic interactions and release the drug payload i) intracellularly by fusion of the liposome with the cell membrane or ii) in the extracellular fluid by degradation of the lipid bilayer upon contact with the cell membrane (enzymes such as lipases or mechanical forces may be involved).<sup>33</sup> Furthermore, the analysis of LGR5 expression by flow cytometry carried out by Vázquez-Iglesias et al revealed 22.5, 8.0 and 9.1% of LGR5+ cells in T84, SW480, and HT29 cell lines, respectively.<sup>45</sup> Therefore, it would be interesting to develop new targeting strategies using multiple CRC biomarkers such as the bispecific antibody MCLA-158 anti-LGR5 and EGFR which inhibited the growth of KRAS-mutated CRC and suppressed the development of metastasis in epithelial tumors.<sup>24</sup>

Finally, some studies have described in vivo toxic effects of iron oxide nanoparticles administered by distinct routes on healthy tissues such as the liver<sup>46,47</sup> and spleen,<sup>48</sup> among others<sup>49</sup> that could be overcome or reduced with magnetoliposome use. Our results showed no signs of toxicity in terms of mice and organs’ weight with the treatment of unloaded magnetoliposomes except with BML2 treatment. Hepatic iron deposits were visualized by Prussian blue iron staining without the presence of liver tissue damage, and no abnormalities in liver enzymes were observed except

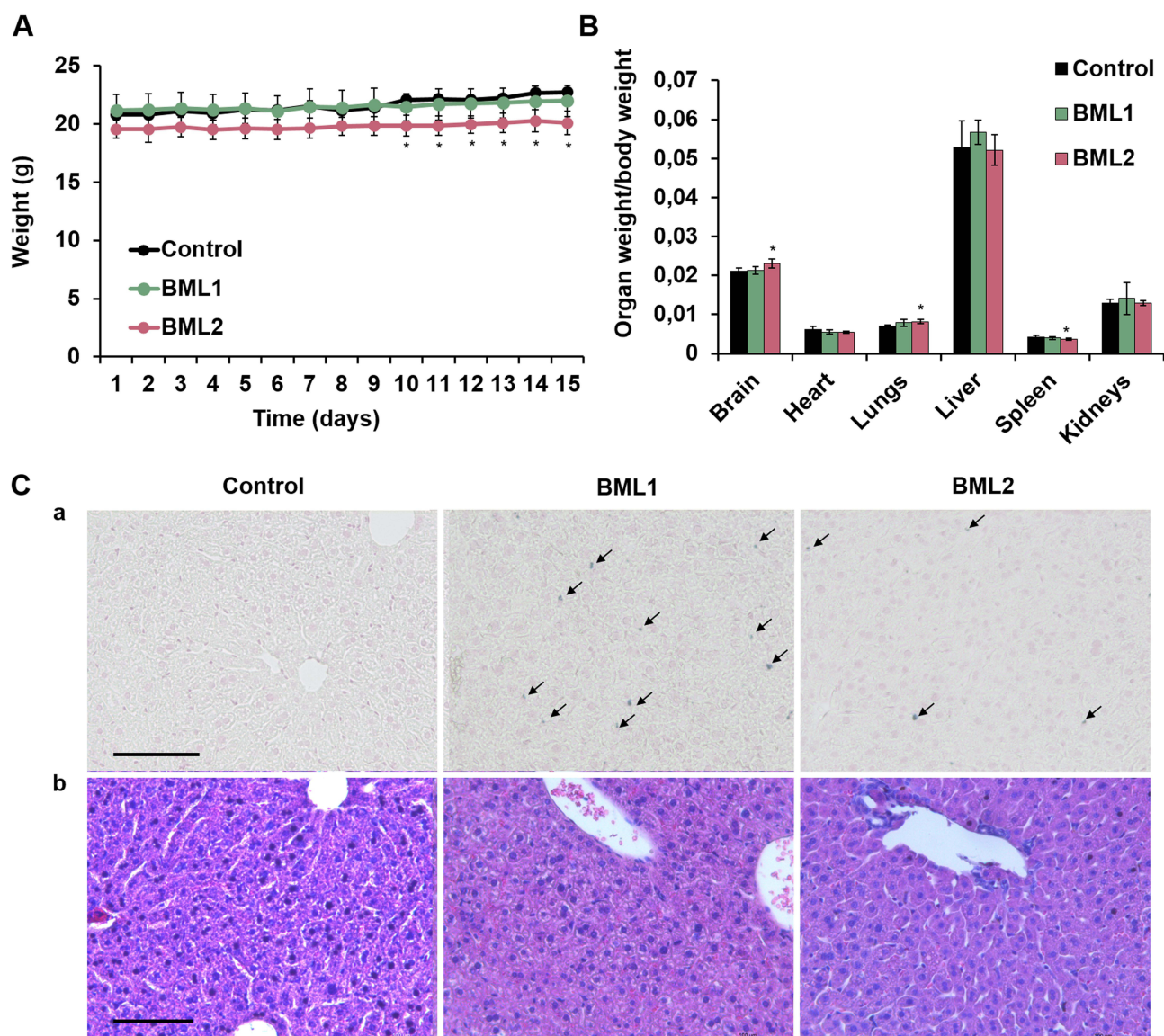


**Figure 12** Acute toxicity of Fe in mice treated with BML1 and BML2. **(A)** Body weight variation along the experiment and **(B)** weight of mice organs at the endpoint of the experiment. Data represented mean  $\pm$  SD ( $n = 16$ ). (\*) P-value  $< 0.05$  compared to control mice and determined by one-way repeated measures ANOVA and Student's *t*-test, respectively. **(C)** Stained (a) Prussian blue (b) hematoxylin & eosin liver samples from untreated and BML1 and 2 treated mice. Iron accumulations are marked with black arrows. Scale Bar 100  $\mu$ m.

reduced ALP values in BML2-treated group. Although alkaline phosphatase enzyme is measured to detect liver or bone toxicity, a relation to liver disease has only been described when values are increased and not decreased.<sup>50–52</sup> Furthermore, there was no alteration of other biochemical parameters and the majority of blood populations analyzed remained stable compared to the untreated control. Only, a slight increase in hematocrit, as well as eosinophils, can be observed with exposure to both BML1 and BML2 nanoformulations, which had already been described by Askri et al with an increase in the number of red blood cells, hemoglobin, and eosinophils with low doses of iron oxide nanoparticles.<sup>46</sup> Furthermore, the analysis of blood populations showed a decrease in the percentage of macrophages, which is only significant in mice treated with BML1, and an increase in the percentage of neutrophils for BML2 treatment. Moreover, no mortality was observed, and the overall health status of the mice treated with the nanoformulations was not affected compared to the untreated control.

**Table 3** Biochemical Parameters of the Blood Plasma of Mice Treated with BML1 and BML2

Plasma Biochemical Parameter	Control	BML1	BML2
Albumin (g/dL)	2.91 ± 0.18	3.01 ± 0.07	2.92 ± 0.11
Creatinine (mg/dL)	0.16 ± 0.11	0.16 ± 0.06	0.22 ± 0.09
GOT (U/L)	73.20 ± 11.67	98.69 ± 34.43	50.70 ± 36.04
GPT (U/L)	20.57 ± 2.96	25.19 ± 6.61	25.42 ± 6.39
GGT (U/L)	19.72 ± 0.69	18.84 ± 0.85	23.33 ± 7.19
ALP (U/L)	110.76 ± 8.79	70.55 ± 33.43	48.62 ± 7.26 *
Direct bilirubin (mg/dL)	0.06 ± 0.03	0.04 ± 0.02	0.05 ± 0.00
Total bilirubin (mg/dL)	0.12 ± 0.04	0.19 ± 0.06	0.16 ± 0.03
Total proteins (g/dL)	4.94 ± 0.30	5.14 ± 0.30	5.03 ± 0.31
Urea (mg/dL)	67.98 ± 15.57	60.80 ± 10.38	48.10 ± 5.30

**Notes:** Data represented mean ± SD. (\*) P-value < 0.05 compared to control mice determined by Student's t-test.

**Abbreviations:** GOT, glutamic-oxaloacetic transaminase; GPT, glutamate pyruvate transaminase; GTT, gamma-glutamyl transferase, ALP, alkaline phosphatase.

**Table 4** Blood Populations in Mice Treated with BML1 and BML2

Test	Control	BML1	BML2
Total number of WBC (10 <sup>3</sup> /μL)	4.63 ± 1.31	3.3 ± 0.94 *	3.79 ± 0.79
Total number of RBC (10 <sup>6</sup> /μL)	8.28 ± 1.08	8.89 ± 0.58	8.59 ± 1.18
Hemoglobin (g/dL)	13.16 ± 1.68	14.01 ± 0.86	14.32 ± 0.70*
Hematocrit (%)	38.46 ± 5.15	40.98 ± 2.85*	41.4 ± 2.52*
Total number of platelets (10 <sup>3</sup> /μL)	345.25 ± 227.39	361.25 ± 287.25	447 ± 162.79
Lymphocytes (%)	94.99 ± 1.21	94.42 ± 2.11	92.33 ± 3.09*
Monocytes/macrophages (%)	0.34 ± 0.18	0.18 ± 0.08*	0.19 ± 0.15
Neutrophils/polymorphonuclears (%)	4.14 ± 1.18	4.58 ± 1.80	6.13 ± 2.60*
MCV	46.43 ± 1.38	46.09 ± 0.52	46.53 ± 0.96
MCH	15.9 ± 0.41	15.76 ± 0.43	16.05 ± 0.18
MCHC (g/dL)	34.25 ± 0.58	34.23 ± 1.02	34.51 ± 0.59
RBC size distribution	14.35 ± 0.22	14.6 ± 0.38	14.43 ± 0.33
MPV (fL)	5.91 ± 0.27	7 ± 1.51	5.84 ± 0.18
Thrombocrit (%)	0.2 ± 0.12	0.22 ± 0.16	0.27 ± 0.08
Platelet size distribution	27.71 ± 6.55	27.91 ± 8.72	22.68 ± 5.65
Eosinophils (%)	0.14 ± 0.11	0.47 ± 0.31*	0.69 ± 0.40*
Basophils (%)	0.4 ± 0.26	0.37 ± 0.24	0.65 ± 0.30

**Note:** Data represented mean ± SD. (\*) P-value < 0.05 compared to control mice determined by Student's t-test.

**Abbreviations:** WBC, white blood cells; RBC, red blood cells; MCV, mean corpuscular volume; MCH, mean corpuscular hemoglobin; MCHC, mean corpuscular hemoglobin concentration; MPV, mean platelet volume.

## Conclusion

Functionalization with anti-LGR5 antibody of OXA and 5-FU-loaded magnetoliposomes has been successfully conducted, resulting in BML1-OXA-LGR5 and BML2-5-FU-LGR5 nanoformulations. All colorectal cancer cell lines were tested and the control hepatocarcinoma cell line HepG2 exhibited LGR5 positive expression. A murine cell line transduced with shRNA lentiviral particles with reduced LGR5 expression (MC38-L(-)) was established from the murine CRC cell line MC38. OXA or 5FU-loaded BML-LGR5 reduced or maintained the IC<sub>50</sub> value of untargeted magnetoliposomes in CRC cells, accentuating these differences at short exposure times and correlated with higher cell uptake of LGR5-functionalized BMLs in T84, MC38 and MC38-L(-) cell lines with a location mainly cytoplasmic. The differences between the MC38 and the MC38-L(-) could demonstrate cellular uptake mediated by ligand-receptor interaction, although other mechanisms could also be involved.

Moreover, in vivo acute toxicity assay of iron showed good biocompatibility of magnetoliposomes with no deaths or relevant signs of toxicity. Thus, OXA or 5-FU-loaded BMLs targeted with anti-LGR5 antibody could be a new strategy for the targeted therapy of CRC that could be combined with magnetic hyperthermia, specially addressed to LGR5+ cells that seem to be involved in tumor recurrence and chemoresistance.

## Ethics Approval

The in vivo experiment was approved by the Research Ethics Committee of Granada University (Reference code: 07/03/2022/023) and in accordance with international standards (European Communities Council Directive 2010/63).

## Acknowledgments

A.C and M.J.-C., wants to acknowledge FPU2019 and FPU2021, grants (refs. FPU19/04112, and FPU21/01529) from the Ministerio de Universidades (Spain), and C.L. a P-FIS (PI20-00284) from the Ministerio de Ciencia, Innovación y Universidades (Spain). L.G. wants to acknowledge the Junta de Andalucía 2021 Scholarship (ref. PREDOC\_00199) from the “Secretaría General de Universidades, Investigación y Tecnología”, C.J-L. thanks UCE-PP2016-05 and Biotechnology Institute (University of Granada).

## Author Contributions

All authors made a significant contribution to the work reported, whether that is in the conception, study design, execution, acquisition of data, analysis and interpretation, or in all these areas; took part in drafting, revising or critically reviewing the article; gave final approval of the version to be published; have agreed on the journal to which the article has been submitted; and agree to be accountable for all aspects of the work.

## Funding

This research was funded by Project “PI19/01478-FEDER”, funded by Instituto de Salud Carlos III (ISCIII) and co-funded by the European Union, Junta de Andalucía (P20\_00208), FEDER Operational Program (B-BIO-432-UGR20) and Project PDC2021-121135.100 funded through MCIN/AEI/10.13039/501100011033 and the European Union Next GenerationEU/ PRTR. This research was also funded in part by Personalized Medicine and Advanced Therapies Program (PMPTA22/00136), Instituto de Salud Carlos III.

## Disclosure

Dr Concepcion Jimenez-Lopez reports a patent pending PCT/ES2097070747. The authors declare no other conflicts of interest in this work.

## References

1. Biller LH, Schrag D. Diagnosis and Treatment of Metastatic Colorectal Cancer: a Review. *JAMA*. 2021;325(7):669–685. doi:10.1001/JAMA.2021.0106
2. Siegel RL, Miller KD, Goding Sauer A, et al. Colorectal cancer statistics, 2020. *CA Cancer J Clin*. 2020;70(3):145–164. doi:10.3322/CAAC.21601
3. Zafar A, Drobní ZD, Lei M, et al. The efficacy and safety of cardio-protective therapy in patients with 5-FU (Fluorouracil) associated coronary vasospasm. *PLoS One*. 2022;17:1–10. doi:10.1371/journal.pone.0265767
4. Boyne DJ, O’Sullivan DE, Heer EV, et al. Prognostic factors of adjuvant chemotherapy discontinuation among stage III colon cancer patients: a survey of medical oncologists and a systematic review and meta-analysis. *Cancer Med*. 2020;9(5):1613–1627. doi:10.1002/CAM4.2843
5. Kang L, Tian Y, Xu S, Chen H. Oxaliplatin-induced peripheral neuropathy: clinical features, mechanisms, prevention and treatment. *J Neurol*. 2021;268(9):3269–3282. doi:10.1007/S00415-020-09942-W
6. Shukla A, Maiti P. Nanomedicine and versatile therapies for cancer treatment. *MedComm*. 2022;3:3. doi:10.1002/mco.2163
7. Pérez-Herrero E, Fernández-Medarde A. Advanced targeted therapies in cancer: drug nanocarriers, the future of chemotherapy. *Eur J Pharm Biopharm*. 2015;93:52–79. doi:10.1016/J.EJPB.2015.03.018
8. Al-Zoubi MS, Al-Zoubi RM. Nanomedicine tactics in cancer treatment: challenge and hope. *Crit Rev Oncol Hematol*. 2022;174:103677. doi:10.1016/J.CRITREVONC.2022.103677
9. Valverde-Tercedor C, Montalbán-López M, Perez-Gonzalez T, et al. Size control of in vitro synthesized magnetite crystals by the MamC protein of *Magnetococcus marinus* strain MC-1. *Appl Microbiol Biotechnol*. 2015;99(12):5109–5121. doi:10.1007/S00253-014-6326-Y/FIGURES/4
10. García Rubia G, Peigneux A, Jabalera Y, et al. PH-dependent adsorption release of doxorubicin on mamc-biomimetic magnetite nanoparticles. *Langmuir*. 2018;34(45):13713–13724. doi:10.1021/ACS.LANGMUIR.8B03109/ASSET/IMAGES/LARGE/LA-2018-03109E\_0006.JPG

11. Peigneux A, Oltolina F, Colangelo D, et al. Functionalized biomimetic magnetic nanoparticles as effective nanocarriers for targeted chemotherapy. *Part Part Syst Charact.* 2019;36(6):1900057. doi:10.1002/PPSC.201900057
12. Oltolina F, Peigneux A, Colangelo D, et al. Biomimetic magnetite nanoparticles as targeted drug nanocarriers and mediators of hyperthermia in an experimental cancer model. *Cancers.* 2020;12(9):1–25. doi:10.3390/CANCERS12092564
13. Iglesias GR, Jabalera Y, Peigneux A, Fernández BLC, Delgado ÁV, Jimenez-Lopez C. Enhancement of magnetic hyperthermia by mixing synthetic inorganic and biomimetic magnetic nanoparticles. *Pharmaceutics.* 2019;11(6):273. doi:10.3390/PHARMACEUTICS11060273
14. Jabalera Y, Fernández-Vivas A, Iglesias GR, Delgado ÁV, Jimenez-Lopez C. Magnetoliposomes of mixed biomimetic and inorganic magnetic nanoparticles as enhanced hyperthermia agents. *Colloids Surf B Biointerfaces.* 2019;183:110435. doi:10.1016/J.COLSURFB.2019.110435
15. Jabalera Y, Oltolina F, Peigneux A, et al. Nanoformulation design including mmmc-mediated biomimetic nanoparticles allows the simultaneous application of targeted drug delivery and magnetic hyperthermia. *Polymers (Basel).* 2020;12(8):1832. doi:10.3390/POLYM12081832
16. Jabalera Y, Garcia-Pinel B, Ortiz R, et al. Oxaliplatin-biomimetic magnetic nanoparticle assemblies for colon cancer-targeted chemotherapy: an in vitro study. *Pharmaceutics.* 2019;11:8. doi:10.3390/PHARMACEUTICS11080395
17. Garcia-Pinel B, Jabalera Y, Ortiz R, et al. Biomimetic magnetoliposomes as oxaliplatin nanocarriers: in vitro study for potential application in colon cancer. *Pharmaceutics.* 2020;12(6):1–20. doi:10.3390/PHARMACEUTICS12060589
18. Chen R, Huang Y, Wang L, et al. Cetuximab functionalization strategy for combining active targeting and antimigration capacities of a hybrid composite nanoplateform applied to deliver 5-fluorouracil: toward colorectal cancer treatment. *Biomater Sci.* 2021;9(6):2279–2294. doi:10.1039/D0BM01904F
19. Andrade F, Rafael D, Vilar-Hernández M, et al. Polymeric micelles targeted against CD44v6 receptor increase niclosamide efficacy against colorectal cancer stem cells and reduce circulating tumor cells in vivo. *J Control Release.* 2021;331:198–212. doi:10.1016/J.JCONREL.2021.01.022
20. He F, Wen N, Xiao D, et al. Aptamer-based targeted drug delivery systems: current potential and challenges. *Curr Med Chem.* 2020;27(13):2189–2219. doi:10.2174/0929867325666181008142831
21. Tarudji AW, Kievit FM. Active targeting and transport. In: Chung EJ, Leon L editors. *Nanoparticles for Biomedical Applications.* Elsevier; 2020:19–36. doi:10.1016/B978-0-12-816662-8.00003-5
22. Xu N, Gao K, Luo H, Wu Y, Shen B, Liu K. Correlation of Lgr5 expression with clinicopathological features of colorectal cancer and its diagnostic and prognostic values. *J BUON.* 2021;26(1):87–92.
23. Cao J, Li C, Wei X, et al. Selective targeting and eradication of LGR5 + cancer stem cells using RSPO-conjugated doxorubicin liposomes. *Mol Cancer Ther.* 2018;17(7):1475–1485. doi:10.1158/1535-7163.MCT-17-0694/86842/AM/SELECTIVE-TARGETING-AND-ERADICATION-OF-LGR5-CSCS
24. Herpers B, Eppink B, James MI, et al. Functional patient-derived organoid screenings identify MCLA-158 as a therapeutic EGFR × LGR5 bispecific antibody with efficacy in epithelial tumors. *Nat Cancer.* 2022;3(4):418–436. doi:10.1038/S43018-022-00359-0
25. Carina Biotech Limited. A Study of CNA3103 (LGR5-targeted, Autologous CAR-T Cells) administered to subjects with metastatic colorectal cancer. Available from: <https://clinicaltrials.gov/study/NCT05759728>. Accessed December 5, 2023.
26. Martin JD Using X Powder: a software package for powder X-ray diffraction analysis; 2004. Available from: [www.xpowder.com](http://www.xpowder.com). Accessed February 12, 2024.
27. Garcés V, González A, Gálvez N, et al. Magneto-optical hyperthermia agents based on probiotic bacteria loaded with magnetic and gold nanoparticles. *Nanoscale.* 2022;14(15):5716. doi:10.1039/D1NR08513A
28. Schindelin J, Arganda-Carreras I, Frise E, et al. Fiji: an open-source platform for biological-image analysis. *Nat Methods.* 2012;9(7):676–682. doi:10.1038/nmeth.2019
29. Ortiz R, Cabeza L, Arias JL, et al. Poly(butylcyanoacrylate) and Poly( $\epsilon$ -caprolactone) nanoparticles loaded with 5-fluorouracil increase the cytotoxic effect of the drug in experimental colon cancer. *AAPS J.* 2015;17(4):918–929. doi:10.1208/S12248-015-9761-5
30. Tomitaka A, Takemura Y, Huang Z, Roy U, Nair M. Magnetoliposomes in controlled-release drug delivery systems. *Crit Rev Biomed Eng.* 2019;47(6):495–505. doi:10.1615/CRITREVBIOEMEDENG.2020033002
31. Liu P, Chen G, Zhang J. A review of liposomes as a drug delivery system: current status of approved products, regulatory environments, and future perspectives. *Molecules.* 2022;27(4). doi:10.3390/MOLECULES27041372
32. Bhattacharya S, Saindane D, Prajapati BG. Liposomal drug delivery and its potential impact on cancer research. *Anticancer Agents Med Chem.* 2022;22(15):2671–2683. doi:10.2174/1871520622666220418141640
33. Bozzuto G, Molinari A. Liposomes as nanomedical devices. *Int J Nanomed.* 2015;10(1):975–999. doi:10.2147/IJN.S68861
34. Donahue ND, Acar H, Wilhelm S. Concepts of nanoparticle cellular uptake, intracellular trafficking, and kinetics in nanomedicine. *Adv Drug Deliv Rev.* 2019;143:68–96. doi:10.1016/J.ADDR.2019.04.008
35. De Sousa E Melo F, Kurtova AV, Harnoss JM, et al. A distinct role for Lgr5 + stem cells in primary and metastatic colon cancer. *Nature.* 2017;543(7647):676–680. doi:10.1038/nature21713
36. Mao X, Zhang X, Zheng X, Chen Y, Xuan Z, Huang P. Curcumin suppresses LGR5(+) colorectal cancer stem cells by inducing autophagy and via repressing TFAP2A-mediated ECM pathway. *J Nat Med.* 2021;75(3):590. doi:10.1007/S11418-021-01505-1
37. Kondo M, Araie M. Iontophoresis of 5-fluorouracil into the conjunctiva and sclera. *Invest Ophthalmol Vis Sci.* 1989;30(3):583–585.
38. Liang B, Shahbaz M, Wang Y, et al. Integrin $\beta$ 6-targeted immunoliposomes mediate tumor-specific drug delivery and enhance therapeutic efficacy in colon carcinoma. *Clin Cancer Res.* 2015;21(5):1183–1195. doi:10.1158/1078-0432.CCR-14-1194
39. Corvo ML, Mendo AS, Figueiredo S, et al. Liposomes as Delivery System of a Sn(IV) complex for cancer therapy. *Pharm Res.* 2016;33(6):1351–1358. doi:10.1007/s11095-016-1876-6
40. Dadashi Noshahr K, Shamsi F, Valtchev P, et al. Optimization of post-insertion method to conjugate Doxil with anti-CD133 monoclonal antibodies: investigating the specific binding and cytotoxicity to colorectal cancer cells in vitro. *Saudi Pharm J.* 2020;28(11):1392. doi:10.1016/J.JSPS.2020.09.003
41. Park S, Wu L, Tu J, et al. Unlike LGR4, LGR5 potentiates Wnt- $\beta$ -catenin signaling without sequestering E3 ligases. *Sci Signal.* 2020;13(660). doi:10.1126/SCISIGNAL.AAZ4051
42. Jabalera Y, Sola-Leyva A, Peigneux A, et al. Biomimetic magnetic nanocarriers drive choline kinase alpha inhibitor inside cancer cells for combined chemo-hyperthermia therapy. *Pharmaceutics.* 2019;11(8):408. doi:10.3390/PHARMACEUTICS11080408

43. Lubart Q, Hannestad JK, Pace H, et al. Lipid vesicle composition influences the incorporation and fluorescence properties of the lipophilic sulphonated carbocyanine dye SP-DiO. *Phys Chem Chem Phys*. 2020;22(16):8781–8790. doi:10.1039/C9CP04158C
44. Montero S, Seras-Franzoso J, Andrade F, et al. Intracellular delivery of anti-SMC2 antibodies against cancer stem cells. *Pharmaceutics*. 2020;12(2). doi:10.3390/pharmaceutics12020185
45. Vázquez-Iglesias L, Barcia-Castro L, Rodríguez-Quiroga M, De La Cadena MP, Rodríguez-Berrocal J, Cordero OJ. Surface expression marker profile in colon cancer cell lines and sphere-derived cells suggests complexity in CD26 + cancer stem cells subsets. *Biol Open*. 2019;8(7). doi:10.1242/BIO.041673
46. Askri D, Ouni S, Galai S, et al. Nanoparticles in foods? A multiscale physiopathological investigation of iron oxide nanoparticle effects on rats after an acute oral exposure: trace element biodistribution and cognitive capacities. *Food Chem Toxicol*. 2019;127:173–181. doi:10.1016/J.FCT.2019.03.006
47. Salimi M, Sarkar S, Fathi S, et al. Biodistribution, pharmacokinetics, and toxicity of dendrimer-coated iron oxide nanoparticles in BALB/c mice. *Int J Nanomed*. 2018;13:1483–1493. doi:10.2147/IJN.S157293
48. Awaad A. Histopathological and immunological changes induced by magnetite nanoparticles in the spleen, liver and genital tract of mice following intravaginal instillation. *JOBAZ*. 2015;71:32–47. doi:10.1016/J.JOBAZ.2015.03.003
49. Chrishtop VV, Mironov VA, Prilepskii AY, Nikonorova VG, Vinogradov VV. Organ-specific toxicity of magnetic iron oxide-based nanoparticles. *Nanotoxicology*. 2021;15(2):167–204. doi:10.1080/17435390.2020.1842934
50. Sadeghi L, Yousefi Babadi V, Espanani HR. Toxic effects of the Fe<sub>2</sub>O<sub>3</sub> nanoparticles on the liver and lung tissue. *Bratisl Lek Listy*. 2015;116(6):373–378. doi:10.4149/BLL\_2015\_071
51. Parivar K, Fard FM, Bayat M, Alavian SM, Motavaf M. Evaluation of iron oxide nanoparticles toxicity on liver cells of BALB/c rats. *Iran Red Crescent Med J*. 2016;18(1):28939. doi:10.5812/IRCMJ.28939
52. Almanaa TN, Aref M, Kakakhel MA, et al. Silica nanoparticle acute toxicity on male rattus norvegicus domestica: ethological behavior, hematological disorders, biochemical analyses, hepato-renal function, and antioxidant-immune response. *Front Bioeng Biotechnol*. 2022;10:1. doi:10.3389/FBIOE.2022.868111

International Journal of Nanomedicine

Dovepress

## Publish your work in this journal

The International Journal of Nanomedicine is an international, peer-reviewed journal focusing on the application of nanotechnology in diagnostics, therapeutics, and drug delivery systems throughout the biomedical field. This journal is indexed on PubMed Central, MedLine, CAS, SciSearch<sup>®</sup>, Current Contents<sup>®</sup>/Clinical Medicine, Journal Citation Reports/Science Edition, EMBase, Scopus and the Elsevier Bibliographic databases. The manuscript management system is completely online and includes a very quick and fair peer-review system, which is all easy to use. Visit <http://www.dovepress.com/testimonials.php> to read real quotes from published authors.

Submit your manuscript here: <https://www.dovepress.com/international-journal-of-nanomedicine-journal>